

Nucleon Polarisabilities At and Beyond Physical Pion Masses

Harald W. Griebhammer^{a1}, Judith A. McGovern^{b2} and Daniel R. Phillips^{c3}

^a *Institute for Nuclear Studies, Department of Physics,
The George Washington University, Washington DC 20052, USA*

^b *School of Physics and Astronomy, The University of Manchester,
Manchester M13 9PL, UK*

^c *Department of Physics and Astronomy and Institute of Nuclear and Particle Physics,
Ohio University, Athens, Ohio 45701, USA*

Abstract

We examine the results of Chiral Effective Field Theory (χ EFT) for the scalar- and spin-dipole polarisabilities of the proton and neutron, both for the physical pion mass and as a function of m_π . This provides chiral extrapolations for lattice-QCD polarisability computations. We include both the leading and sub-leading effects of the nucleon's pion cloud, as well as the leading ones of the $\Delta(1232)$ resonance and its pion cloud. The analytic results are complete at N²LO in the δ -counting for pion masses close to the physical value, and at leading order for pion masses similar to the Delta-nucleon mass splitting. In order to quantify the truncation error of our predictions and fits as 68% degree-of-belief intervals, we use a Bayesian procedure recently adapted to EFT expansions. At the physical point, our predictions for the spin polarisabilities are, within respective errors, in good agreement with alternative extractions using experiments and dispersion-relation theory. At larger pion masses we find that the chiral expansion of all polarisabilities becomes intrinsically unreliable as m_π approaches about 300 MeV—as has already been seen in other observables. χ EFT also predicts a substantial isospin splitting above the physical point for both the electric and magnetic scalar polarisabilities; and we speculate on the impact this has on the stability of nucleons. Our results agree very well with emerging lattice computations in the realm where χ EFT converges. Curiously, for the central values of some of our predictions, this agreement persists to much higher pion masses. We speculate on whether this might be more than a fortuitous coincidence.

Suggested Keywords: Effective Field Theory, lattice QCD, chiral extrapolation, proton, neutron and nucleon polarisabilities, spin polarisabilities, Chiral Perturbation Theory, $\Delta(1232)$ resonance, Bayesian statistics, uncertainty/error estimates.

¹Email: hgrie@gwu.edu

²Email: judith.mcgovern@manchester.ac.uk

³Email: phillips@phy.ohiou.edu

1 Introduction

The polarisabilities of a composite system are among its most basic properties; see e.g. [1] for a recent review. At a classical level, they reflect how much freedom charged constituents have to rearrange under the application of external electromagnetic fields, while in quantum mechanics they indicate how easily electromagnetic interactions induce transitions to low-lying excited states. They therefore encode information about the symmetries and strengths of constituents’ interactions with each other and with the photon. As well as the usual electric (α_{E1}) and magnetic (β_{M1}) polarisabilities, a spin-half object like the nucleon has four “spin-polarisabilities” (γ_i). These are less obvious in their effects but encode the spin-dependent response and can, for instance, be related to effects analogous to birefringence and Faraday rotation for long-wavelength electromagnetic radiation. In the nucleon, the lightest relevant excitation involves the creation of a virtual charged pion. This mechanism is expected to dominate the electric polarisability and contribute significantly to others, too. The exploration of nucleon polarisabilities was therefore a natural early application of Chiral Perturbation Theory in the baryonic sector [2–4] which predicts the behaviour of each polarisability as it diverges in the chiral limit $m_\pi \rightarrow 0$ [3]. On the other hand, in the real world the excitation energy of the $\Delta(1232)$ resonance, $\Delta_M \equiv M_\Delta - M_N$, is about 300 MeV, and thus not very much larger than the physical pion mass. Furthermore, the strong magnetic $N\Delta$ dipole transition should give a large paramagnetic contribution to the magnetic polarisability.

The inclusion of the Delta as an explicit degree of freedom in Chiral Effective Field Theory [2, 5–7] enables quantitative predictions to be made for Compton scattering [8, 9]. This EFT has recently been used in the most accurate extant determinations of the electric and magnetic polarisabilities of the proton and neutron from Compton scattering data [1, 10, 11]. This progress in the theory of polarisabilities is coupled to an upsurge of interest in new experiments that are devoted to obtaining or refining our knowledge of all the polarisabilities, electric, magnetic and spin, of both the proton and neutron [12–15], with results from MAXlab [11, 16] and MAMI [17] published within the last year.

The calculation of nucleon polarisabilities directly from the QCD action is also an aim of lattice QCD. The need to incorporate electromagnetic fields in the computation creates challenges, which means that this is a fairly new endeavour, but several groups now have published results [18–27]. Since all are at pion masses substantially above the physical pion mass, the question of how to extrapolate to the real world is of pressing interest, and can be addressed within χ EFT. Our analysis provides a bridge between data and lattice QCD, where a direct computation of Compton scattering would be highly nontrivial.

Polarisabilities are therefore fundamental characteristics of hadrons, and benchmarks for our understanding of hadronic structure; a summary of their importance and best ways to access them was also provided by a number of theorists in Ref. [28]. Furthermore, their values have other implications, some examples of which we now discuss. First, the Cottingham Sum rule relates the doubly-virtual forward Compton scattering amplitude, and hence the proton-neutron difference in β_{M1} , to the proton-neutron electromagnetic mass difference [29–33]. The relation between the mass difference and the polarisabilities pro-

ceeds via a low-energy theorem for the subtraction function in the Cottingham formula at vanishing momentum, which is related to $\beta_{M1}^{(p-n)}$ [29, 33]. When one uses present knowledge on $\beta_{M1}^{(p-n)}$ as input and models the subtraction function along the lines suggested in Refs. [29–31], the uncertainty in the polarisability contributes sizeably to the uncertainty in the mass difference. Conversely, assuming knowledge about the electromagnetic part of the mass difference provides a constraint on the polarisabilities [32]. Either scenario tests our understanding of the subtle interplay between electromagnetic and strong interactions in a fundamental observable. Second, the magnetic polarisability, β_{M1} , is also crucial for the two-photon-exchange contribution to the Lamb shift in muonic hydrogen [34–36], the least-known ingredient of the “proton-radius puzzle”.

The aim of this paper is thus two-fold. Firstly, we will present the analytic expressions and numerical results for all static dipole polarisabilities as they enter in the Compton amplitudes used in the recent proton and neutron analyses [10, 11]. There is considerable evidence that the extraction of $\alpha_{E1}^{(p)}$ and $\beta_{M1}^{(p)}$ from unpolarised Compton scattering is robust against variations in the spin polarisabilities [1, 10, 37]. This means that polarisation observables are the best place to determine these latter quantities [38], and programs at MAMI and HI γ S are engaged in that pursuit [12–15]. Secondly, we use our expressions to predict the running of the polarisabilities with the pion mass, the better to compare with lattice computations at numerically less costly, heavier, pion masses.

In both these contexts, we pay particular attention to the uncertainties of our predictions and extractions, which are of two types. The impact of statistical errors on data on χ EFT parameters can ultimately be reduced by experimental and non-EFT-related efforts. However, there is also a “truncation error” which is intrinsic to an EFT, and it is that we focus on in this paper. Because χ EFT gives a perturbative series for all polarisabilities, this truncation error accounts for the fact that we only have computed up to a finite order in the EFT expansion [39, 40]. Without its proper appraisal—and that of any other uncertainties entering the χ EFT result—the significance of any agreement or discrepancy between theory and experiment cannot be assessed [41].

On a technical note we mention here that although polarisabilities are frequency-dependent functions (see e.g. [1, 9, 42]), this paper is concerned with the static values, that is the limit as $\omega \rightarrow 0$. We will report these in the canonical units of 10^{-4} fm^3 for the scalar polarisabilities, and 10^{-4} fm^4 for the spin ones. Preliminary findings were reported in Ref. [43] and provided for inclusion in Refs. [17, 19].

The presentation is organised as follows. In Sect. 2, we define the chiral power counting in the regimes relevant for lattice computations and summarise the analytic results for the scalar and spin polarisabilities of the proton and neutron. After presenting their values and uncertainties for physical pion masses in Sect. 3.1, we detail our procedure to assign Bayesian degree-of-belief intervals (Sects. 3.2 and 3.3) and discuss convergence checks. Section 4 extends this procedure to pion masses above the physical point, provides predictions with error bars in Fig. 7, and concludes with speculations on the relationship of our findings to the proton-neutron mass splitting and anthropic arguments. We then compare with available lattice computations in Sect. 5, and add Conclusions and an Appendix.

2 χ EFT with Dynamical $\Delta(1232)$ for Polarisabilities

2.1 Chiral Regimes and Power Counting

Compton scattering on nucleons in χ EFT has been reviewed in Refs. [1, 10], to which we refer the reader for notation and the relevant parts of the chiral Lagrangian. Here, we briefly discuss the power counting, which is crucial for our considerations, and sketch the results.

Recall that Compton scattering exhibits three typical low-energy scales in χ EFT with a dynamical Delta: the pion mass m_π as the typical chiral scale; the Delta-nucleon mass splitting $\Delta_M \approx 300$ MeV; and the photon energy ω . Each provides a small, dimensionless expansion parameter when measured in units of a natural “high” scale $\Lambda_\chi \gg \Delta_M, m_\pi, \omega$ at which the theory is to be expected to break down because new degrees of freedom enter. For static scalar polarisabilities, one considers the part of the amplitude which is quadratic in ω as $\omega \rightarrow 0$, and for spin polarisabilities the one cubic in ω . That leaves two parameters:

$$P(m_\pi) \equiv \frac{m_\pi}{\Lambda_\chi} \quad \epsilon \equiv \frac{M_\Delta - M_N}{\Lambda_\chi} \approx 0.4 \quad , \quad (2.1)$$

where for simplicity we take one common breakdown scale $\Lambda_\chi \approx 650$ MeV for both expansions, consistent with the masses of the ω and ρ as the next-lightest exchange mesons; we also count $M_N \sim \Lambda_\chi$. This scale is only weakly dependent on m_π , and we will treat it as constant.

The fact that these two expansion parameters have a very different functional dependence on m_π has important consequences for chiral extrapolations. The Delta-nucleon mass splitting depends only weakly on the pion mass, and hence ϵ is independent of m_π at the order to which we work. By definition, though, the chiral parameter $P(m_\pi)$ does change significantly with m_π . We therefore identify three regimes relevant in contemporary lattice computations, based on the relative size of P and ϵ . We stress that regimes are not clearly separated, but transition from one regime to the next is gradual.

In **regime (i)**, around the physical pion mass, $m_\pi \approx m_\pi^{\text{phys}}$, we follow Pascalutsa and Phillips [8] and exploit a numerical coincidence to define a single expansion parameter δ :

$$\text{regime (i): } \delta \approx \epsilon \approx \sqrt{P(m_\pi^{\text{phys}})} \approx 0.4 \quad . \quad (2.2)$$

This is, of course, the regime relevant for the analysis of real-world Compton scattering data, and hence this power counting determines the contributions which were included in Refs. [1, 10] which should be consulted for more details.

As the pion mass increases, we move into **regime (ii)**, $m_\pi \approx \Delta_M \approx 300$ MeV. The two expansion parameters are now numerically of comparable size, $P(m_\pi) \approx \epsilon$, but their m_π dependence is still different. It is then appropriate to identify

$$\text{regime (ii): } \epsilon \approx P(m_\pi \approx \Delta_M) \approx 0.4 \quad (2.3)$$

as the sole expansion parameter [2, 5–7].

Finally in **regime (iii)**, $m_\pi \rightarrow \Lambda_\chi$, χ EFT becomes inapplicable because the chiral expansion does not converge. A chiral extrapolation of any observable can be expected to hold qualitatively at best. In Sect. 5, we will see that χ EFT’s polarisabilities agree in the main with extant lattice results at such pion masses, but why this should be so is unclear. The corresponding uncertainties are certainly impossible to quantify with present techniques.

Note that we will not discuss the power counting for very small pion masses, $m_\pi \ll M_\Delta - M_N$. This regime near the chiral limit is fascinating, but it will be some time before lattice computations explore it.

2.2 Dipole Polarisabilities in Regime (i)

Here we bring together the relevant expressions for the various contributions to the polarisabilities: π N loops (calculated to subleading order), $\pi\Delta$ loops, Delta pole diagrams, and low-energy constants from the fourth-order π N Lagrangian. The expressions for the dipole polarisabilities are mostly published, but they are scattered in the literature. The numerical values of all variables are listed in Refs. [1, 10]¹.

When we cite the expressions for all polarisabilities, we are excluding any “non-structure” effects which would persist for a point-like nucleon with an anomalous magnetic moment. For the spin polarisabilities we also exclude the contribution of the π^0 pole [1]. These definitions are standard in the literature, except that the backward spin polarisability γ_π is often given without subtraction of the pion pole contribution of ∓ 45.9 for the proton/neutron. In terms of the multipole polarisabilities, the forward and backward spin polarisabilities are defined as

$$\gamma_0 := -\gamma_{E1E1} - \gamma_{M1M1} - \gamma_{E1M2} - \gamma_{M1E2} \quad , \quad \gamma_\pi := -\gamma_{E1E1} + \gamma_{M1M1} - \gamma_{E1M2} + \gamma_{M1E2} \quad . \quad (2.4)$$

We work in a heavy-baryon framework, except for the Delta pole, whose case is explained shortly. In δ counting, in regime (i), the leading contribution to the Compton scattering amplitudes is the Thomson term which is $\mathcal{O}(e^2)$, followed by leading π N loops which are $\mathcal{O}(e^2\delta^2)$, then diagrams with a single Delta propagator which are $\mathcal{O}(e^2\delta^3)$, and finally subleading π N loops and LECs (counter terms) at $\mathcal{O}(e^2\delta^4)$. In two cases, our expressions also contain terms which are higher-order in δ counting. First, we do not expand the $\pi\Delta$ loop expressions in powers of $m_\pi/\Delta_M \approx \delta$; this has the advantage that the expression remains valid as we move towards regime (ii) $m_\pi \sim \Delta_M$. However, we do omit higher-order graphs that are suppressed by Δ_M/Λ_χ relative to the leading ones. The other exception is that we use a covariant Delta propagator for its pole graphs. Since no loops or renormalisation are involved, this is simply a convenient way of accounting for some kinematic higher-order effects, including the electric $\gamma N\Delta$ coupling, which are relevant in the regime $\omega \sim \Delta_M$. For our present purposes these are not necessary, but as they are small at the physical point and do not affect the running with m_π , we retain them for consistency with our previous work [10].

¹These contain a merely typographical error for $\kappa^{(s)} = -0.12$.

Before presenting the formulae, we note a subtlety which arises when one counts polarisabilities rather than amplitudes. The electric and magnetic polarisabilities α_{E1} and β_{M1} follow the power-counting outlined above; since in the amplitudes they multiply two powers of $\omega \sim m_\pi \sim \delta^2$, the contributions are $\mathcal{O}(e^2\delta^{-2}) \sim m_\pi^{-1}$ from the leading πN pieces, $\mathcal{O}(e^2\delta^{-1}) \sim \Delta_M^{-1}$ from Delta contributions and $\mathcal{O}(e^2\delta^0)$ from subleading πN pieces, generating $\ln m_\pi$ as well as m_π -independent contributions. On the other hand, the spin polarisabilities γ_i multiply three powers of $\omega \sim m_\pi$ and hence start at $\mathcal{O}(e^2\delta^{-4}) \sim m_\pi^{-2}$. However, there are no contributions at $\mathcal{O}(e^2\delta^{-3}) \sim (m_\pi\Delta_M)^{-1}$ since the Delta-nucleon mass difference acts as an infrared cut-off, forbidding Delta contributions to diverge in the chiral limit. Instead, the Delta contributions start at $\mathcal{O}(e^2\delta^{-2}) \sim \Delta_M^{-2}$, and these, together with the subleading pion loops which are $\mathcal{O}(e^2\delta^{-2}) \sim m_\pi^{-1}$, form the next non-zero contribution to the (isoscalar) spin polarisabilities. This has consequences for our error estimates, which are more reliable for α_{E1} and β_{M1} where we have three nonzero terms in the δ expansion series, than they are for the γ_i where there are only two. In either case, the last contribution calculated is of order δ^2 relative to leading.

2.2.1 πN Loops

The leading-order (LO) contributions from the pion cloud around the nucleon, Fig. 1, were first calculated by Bernard, Kaiser and Meißner [3, 4]:

$$\alpha_{E1}^{\pi N, \text{LO}} = 10\beta_{M1}^{\pi N, \text{LO}} = \frac{5\alpha_{\text{EM}}g_A^2}{96\pi f_\pi^2 m_\pi} \quad (2.5)$$

$$\gamma_{E1E1}^{\pi N, \text{LO}} = 5\gamma_{M1M1}^{\pi N, \text{LO}} = -5\gamma_{M1E2}^{\pi N, \text{LO}} = -5\gamma_{E1M2}^{\pi N, \text{LO}} = -\frac{5\alpha_{\text{EM}}g_A^2}{96\pi^2 f_\pi^2 m_\pi^2} \quad (2.6)$$

As motivated above, they diverge in the chiral limit and are indeed $\mathcal{O}(e^2 m_\pi^{-1} \sim e^2 \delta^{-2})$ for the scalar polarisabilities, and $\mathcal{O}(e^2 m_\pi^{-2} \sim e^2 \delta^{-4})$ for the spin ones.

For future reference we note that the π^0 -pole contributes

$$\gamma_{E1E1}^{\pi^0} = -\gamma_{M1M1}^{\pi^0} = \gamma_{E1M2}^{\pi^0} = -\gamma_{M1E2}^{\pi^0} = \tau_3 \frac{e^2 g_{\pi NN}}{16\pi^3 f_\pi M_N m_{\pi^0}^2}, \quad (2.7)$$

where τ_3 is the third Pauli matrix in isospin space. This has the numerical value of 11.5 for the proton at the physical pion mass (with $g_{\pi NN}^2/(4\pi) = 13.64$ [44]).

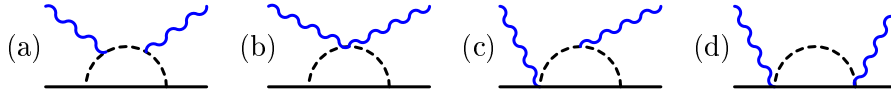


Figure 1: (Colour online) Leading contributions to the polarisabilities from the pion cloud around a nucleon in χ EFT. Interactions without symbol from $\mathcal{L}_{\pi N}^{(1)}$ [4]. Permuted and crossed diagrams not displayed.

The first chiral corrections, shown in Fig. 2, were found by Bernard et al. [45] for the scalar polarisabilities (logarithmic in m_π) and by Kumar, McGovern and Birse [46] for the spin ones (one inverse power of m_π):

$$\begin{aligned}\alpha_{E1}^{\pi N, \text{corr}} &= \frac{\alpha_{\text{EM}}}{24\pi^2 f_\pi^2} \left[\left(\frac{2(3 + \tau_3)g_A^2}{M_N} - c_2 \right) \ln \frac{m_\pi}{m_\pi^{\text{phys}}} + \left(\frac{(27 + 8\tau_3)g_A^2}{4M_N} - (2c_1 + \frac{c_2}{2} - c_3) \right) \right] \\ \beta_{M1}^{\pi N, \text{corr}} &= \frac{\alpha_{\text{EM}}}{24\pi^2 f_\pi^2} \left[\left(\frac{3(2 + (1 + \kappa^{(s)})\tau_3)g_A^2}{M_N} - c_2 \right) \ln \frac{m_\pi}{m_\pi^{\text{phys}}} \right. \\ &\quad \left. + \left(\frac{(13 + 6(1 + \kappa^{(s)})\tau_3)g_A^2}{4M_N} + (2c_1 - \frac{c_2}{2} - c_3) \right) \right]\end{aligned}\quad (2.8)$$

$$\begin{aligned}\gamma_{E1E1}^{\pi N, \text{corr}} &= \frac{\alpha_{\text{EM}} g_A^2}{384\pi f_\pi^2 M_N m_\pi} 11(2 + \tau_3) \\ \gamma_{M1M1}^{\pi N, \text{corr}} &= \frac{\alpha_{\text{EM}} g_A^2}{384\pi f_\pi^2 M_N m_\pi} (15 + 4\kappa^{(v)} + 4(1 + \kappa^{(s)})\tau_3) \\ \gamma_{E1M2}^{\pi N, \text{corr}} &= \frac{\alpha_{\text{EM}} g_A^2}{384\pi f_\pi^2 M_N m_\pi} (-6 - \tau_3) \\ \gamma_{M1E2}^{\pi N, \text{corr}} &= \frac{\alpha_{\text{EM}} g_A^2}{384\pi f_\pi^2 M_N m_\pi} (-1 + 2\kappa^{(v)} - 2(1 + \kappa^{(s)})\tau_3) \quad ,\end{aligned}\quad (2.9)$$

where $\kappa^{(s)} = \kappa^{(p)} + \kappa^{(n)} = -0.12$ and $\kappa^{(v)} = \kappa^{(p)} - \kappa^{(n)} = 3.71$ are the anomalous magnetic moments of the nucleon, and $c_{1,2,3}$ low-energy constants from the next-to-leading order (NLO) πN Lagrangian, determined, e.g. from πN scattering. We set the renormalisation scale in the chiral logarithms to be m_π^{phys} .

To the order we work, these are the *only* m_π -dependent contributions which contain an isovector component and hence differentiate between proton and neutron polarisabilities. For α_{E1} and β_{M1} , the chiral logarithm provides a parameter-free and rather strong m_π -dependence in the difference—besides an m_π -independent offset. The pion-mass dependence of the proton-neutron split in the spin polarisabilities is stronger, scaling with m_π^{-1} , but will turn out to be considerably smaller than the theoretical uncertainties of our predictions. See discussions in Sects. 4.3, 4.4 and 5.

2.2.2 Low-Energy Coefficients

In addition to the loops, there are contributions to polarisabilities directly from the m_π - and Δ_M -independent low-energy coefficients (LECs) multiplying operators in the Lagrangian. Their finite parts subsume physics which is unrelated to the pion cloud or to the Delta, generically:

$$\xi^{\text{LEC}} = \xi^{(s)\text{LEC}} + \tau_3 \xi^{(v)\text{LEC}} \quad (2.10)$$

for the isoscalar and isovector LECs of any polarisability $\xi \in \{\alpha_{E1}, \beta_{M1}, \gamma_i\}$.

Of these, only α_{E1}^{LEC} and β_{M1}^{LEC} need to be included as counter terms at the same order as the πN corrections to α_{E1} and β_{M1} of eqs. (2.8); they absorb the renormalisation-point dependence of the chiral logarithms induced by the divergent loops of Fig. 2.

In Ref. [10], we determined the proton values by fitting to a statistically consistent proton Compton database detailed in Ref. [1]. The results, given in eq. (3.1), are constrained by the Baldin sum rule $\alpha_{E1}^{(p)} + \beta_{M1}^{(p)} = 13.8 \pm 0.4$ [47], though fitting $\alpha_{E1}^{(p)}$ and $\beta_{M1}^{(p)}$ separately produces results which are consistent within the uncertainties. In the same work, it was found that a good fit to (unpolarised) proton Compton scattering data at $\mathcal{O}(e^2\delta^4)$ in the amplitudes could only be achieved if one also determines $\gamma_{M1M1}^{(p)\text{LEC}}$. This makes $\gamma_{M1M1}^{(p)}$ also a fitted quantity.

The neutron scalar polarisabilities are obtained from deuteron targets. In Ref. [11], we extracted scalar polarisabilities for the neutron from the statistically-consistent world data, updated with the recent high-quality data from MAX-lab [16], with the neutron's Baldin sum rule $\alpha_{E1}^{(n)} + \beta_{M1}^{(n)} = 15.2 \pm 0.4$ as a constraint [48]. This extraction was carried out at one order lower, $\mathcal{O}(e^2\delta^3)$, which means that the theoretical uncertainties are larger, but there was no need to fit $\gamma_{M1M1}^{(n)}$. For the sake of the present study, we take a minimalist approach and assume that the γ_{M1M1} LEC we promoted by one order is purely isoscalar, while all other short-distance contributions to the spin polarisabilities enter at higher order. In Sect. 4.3, we will show that the dependence of γ_{M1M1} on the pion mass provides supporting evidence for this.

2.2.3 $\Delta(1232)$ Pole Contribution

Since Δ_M is about 30% of M_N , recoil effects in this part of the amplitude are expected to be sizeable. We thus choose to include purely kinematic, relativistic effects in the Delta pole contribution (see leftmost graph of Fig. 3). The results in Lorentz-covariant kinematics were implicit in Ref. [10], but are stated here for the first time. Related results, but with

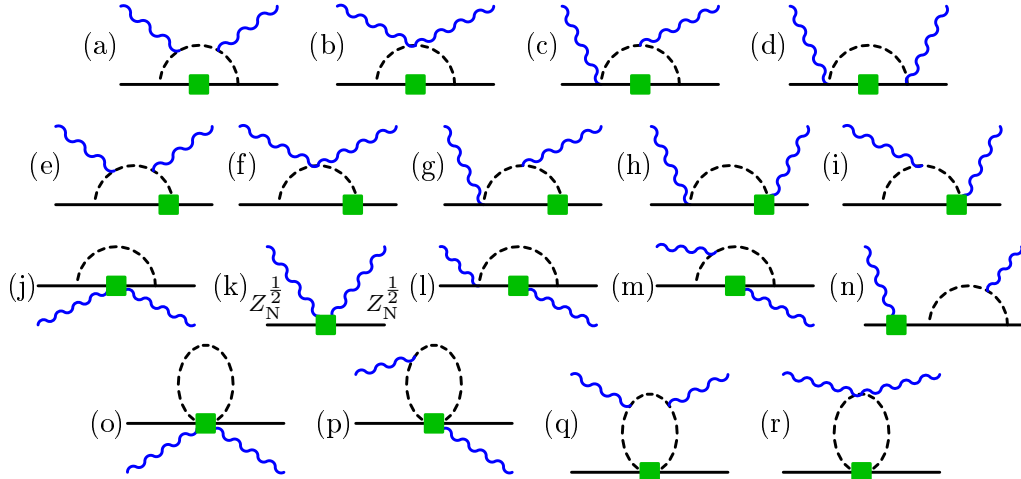


Figure 2: (Colour online) Subleading contributions to the polarisabilities from the pion cloud around a nucleon in χ EFT. Notation as in Fig. 1; square: vertex from $\mathcal{L}_{\pi N}^{(2)}$ [4]. Permuted and crossed diagrams not displayed.

several errors, were given in Ref. [49].

$$\alpha_{E1}^\Delta = -\frac{2\alpha_{\text{EM}}b_2^2}{9M_N^2(2M_N + \Delta_M)} \quad (2.11)$$

$$\begin{aligned} \beta_{M1}^\Delta &= \frac{2\alpha_{\text{EM}}b_1^2}{9M_N^2\Delta_M} \\ \gamma_{E1E1}^\Delta &= \frac{\alpha_{\text{EM}}}{18M_N^3} \left[-\frac{b_1^2}{\Delta_M} + \frac{b_1b_2}{2M_N + \Delta_M} - \frac{2b_2^2(M_N + \Delta_M)}{(2M_N + \Delta_M)^2} \right] \\ \gamma_{M1M1}^\Delta &= \frac{\alpha_{\text{EM}}}{18M_N^3} \left[\frac{2b_1^2(M_N + \Delta_M)}{\Delta_M^2} - \frac{b_1b_2}{\Delta_M} + \frac{b_2^2}{2M_N + \Delta_M} \right] \\ \gamma_{E1M2}^\Delta &= \frac{\alpha_{\text{EM}}}{18M_N^3} \left[-\frac{b_1^2}{\Delta_M} + \frac{3b_1b_2}{2M_N + \Delta_M} \right] \\ \gamma_{M1E2}^\Delta &= \frac{\alpha_{\text{EM}}}{18M_N^3} \left[-\frac{3b_1b_2}{\Delta_M} + \frac{b_2^2}{2M_N + \Delta_M} \right] \end{aligned} \quad (2.12)$$

These contributions reduce at leading order in the heavy-baryon limit, $M_N \rightarrow \infty$ and $b_2 \rightarrow 0$, to the results by Hemmert et al. [50, 51], namely $\gamma_{M1M1}^\Delta = \beta_{M1}^\Delta/(2\Delta_M)$. All other polarisabilities are zero in this limit. Here, b_1 and b_2 are the magnetic and electric $\gamma N\Delta$ couplings respectively. Their leading chiral loop corrections were derived in Ref. [10] but enter an order of $m_\pi/\Lambda_\chi \sim \delta^2$ higher, and are thus omitted from the results above.

2.2.4 $\pi\Delta$ Loops

The leading contributions from the pion cloud around the Delta, Fig. 3, were calculated in Refs. [50, 51] using the heavy-baryon approximation:

$$\alpha_{E1}^{\pi\Delta} = \frac{\alpha_{\text{EM}}g_{\pi N\Delta}^2}{54\pi^2f_\pi^2} \left[\frac{9\Delta_M}{\Delta_M^2 - m_\pi^2} + \frac{\Delta_M^2 - 10m_\pi^2}{(\Delta_M^2 - m_\pi^2)^{\frac{3}{2}}} F\left(\frac{\Delta_M}{m_\pi}\right) \right] \quad (2.13)$$

$$\beta_{M1}^{\pi\Delta} = \frac{\alpha_{\text{EM}}g_{\pi N\Delta}^2}{54\pi^2f_\pi^2} \frac{1}{(\Delta_M^2 - m_\pi^2)^{\frac{1}{2}}} F\left(\frac{\Delta_M}{m_\pi}\right)$$

$$\gamma_{E1E1}^{\pi\Delta} = \frac{\alpha_{\text{EM}}g_{\pi N\Delta}^2}{108\pi^2f_\pi^2} \left[\frac{\Delta_M^2 + 5m_\pi^2}{(\Delta_M^2 - m_\pi^2)^2} + \frac{\Delta_M(\Delta_M^2 - 7m_\pi^2)}{(\Delta_M^2 - m_\pi^2)^{\frac{5}{2}}} F\left(\frac{\Delta_M}{m_\pi}\right) \right] \quad (2.14)$$

$$\gamma_{M1M1}^{\pi\Delta} = -\gamma_{E1M2}^{\pi\Delta} = -\gamma_{M1E2}^{\pi\Delta} = -\frac{\alpha_{\text{EM}}g_{\pi N\Delta}^2}{108\pi^2f_\pi^2} \left[\frac{1}{\Delta_M^2 - m_\pi^2} - \frac{\Delta_M}{(\Delta_M^2 - m_\pi^2)^{\frac{3}{2}}} F\left(\frac{\Delta_M}{m_\pi}\right) \right],$$

with $F(x) = \text{arcsinh}(\sqrt{x^2 - 1})$ and $g_{\pi N\Delta}$ the $\pi N\Delta$ coupling constant. These results are real, continuous and non-singular for all ratios $m_\pi/\Delta_M > 0$.

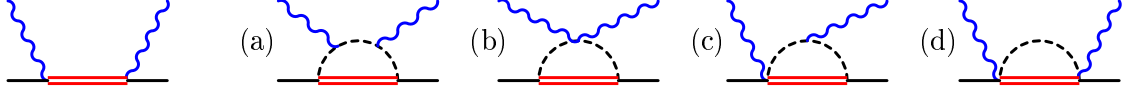


Figure 3: (Colour online) Leading contributions to the polarisabilities from the $\Delta(1232)$ (leftmost) and its pion cloud. Notation as in Fig. 1; covariant $\gamma N\Delta$ and heavy-baryon $\pi N\Delta$ vertices from Ref. [10]. Permuted and crossed diagrams not displayed.

3 Polarisabilities and Uncertainties at the Physical Point

3.1 Summary

The formulae of the previous section with the LECs for $\alpha_{E1}^{(p)}$, $\beta_{M1}^{(p)}$, $\alpha_{E1}^{(n)}$, $\beta_{M1}^{(n)}$ and $\gamma_{M1M1}^{(s)}$ fitted to unpolarised Compton scattering data give the values of the scalar polarisabilities of the nucleons in units of 10^{-4} fm^3 as follows [10, 11]:

$$\begin{aligned}
 \alpha_{E1}^{(p)} &= 10.65 \pm 0.35(\text{stat}) \pm 0.2(\text{Baldin}) \pm 0.3(\text{theory}) \\
 \beta_{M1}^{(p)} &= 3.15 \mp 0.35(\text{stat}) \pm 0.2(\text{Baldin}) \mp 0.3(\text{theory}) \\
 \alpha_{E1}^{(n)} &= 11.55 \pm 1.25(\text{stat}) \pm 0.2(\text{Baldin}) \pm 0.8(\text{theory}) \\
 \beta_{M1}^{(n)} &= 3.65 \mp 1.25(\text{stat}) \pm 0.2(\text{Baldin}) \mp 0.8(\text{theory}) ,
 \end{aligned} \tag{3.1}$$

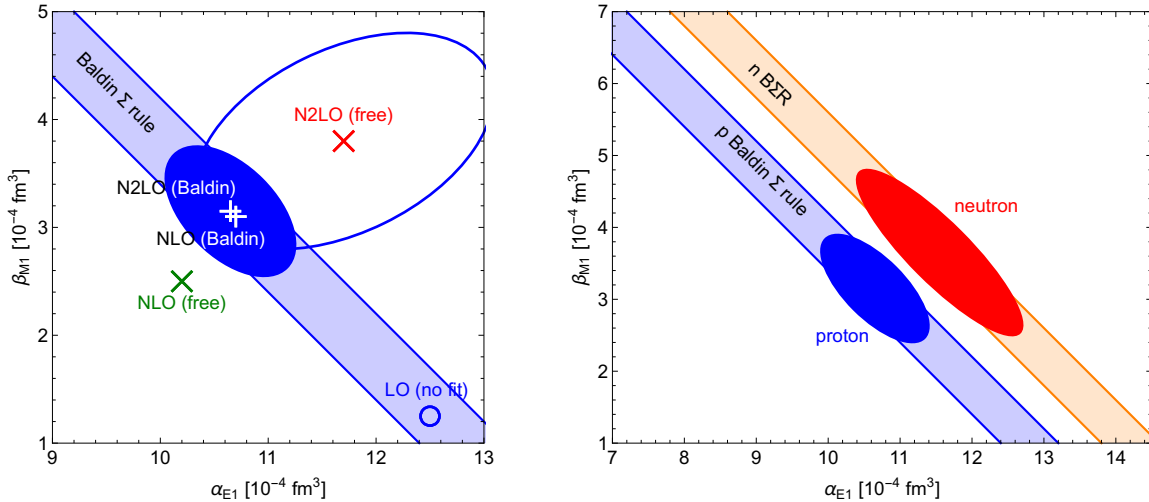


Figure 4: (Colour online) Left: Convergence pattern of the scalar polarisabilities of the proton discussed in Ref. [10], with and without the Baldin sum rule constraint. Ellipses and lines of the $N^2\text{LO}$ determination denote $1\text{-}\sigma$ confidence intervals and account only for experimental errors. Right: Proton and neutron scalar polarisabilities in recent χEFT extractions [10, 11]. Ellipses denote $1\text{-}\sigma$ confidence intervals and add theoretical, experimental/statistical and Baldin-sum-rule related uncertainties in quadrature.

with $\chi^2 = 113.2$ for 135 degrees of freedom for the proton, and 45.2 for 44 for the neutron. Notice that due to the imposition of the Baldin sum rule for each nucleon, both the statistical and theory errors are anticorrelated between α_{E1} and β_{M1} ; see also Sect. 3.3.

For the spin polarisabilities, in units of 10^{-4} fm^4 :

$$\begin{aligned}
\gamma_{E1E1}^{(p)} &= -1.1 \pm 1.9(\text{theory}) & \gamma_{E1E1}^{(n)} &= -4.0 \pm 1.9(\text{theory}) \\
\gamma_{M1M1}^{(p)} &= 2.2 \pm 0.5(\text{stat}) \pm 0.6(\text{theory}) & \gamma_{M1M1}^{(n)} &= 1.3 \pm 0.5(\text{stat}) \pm 0.6(\text{theory}) \\
\gamma_{E1M2}^{(p)} &= -0.4 \pm 0.6(\text{theory}) & \gamma_{E1M2}^{(n)} &= -0.1 \pm 0.6(\text{theory}) \\
\gamma_{M1E2}^{(p)} &= 1.9 \pm 0.5(\text{theory}) & \gamma_{M1E2}^{(n)} &= 2.4 \pm 0.5(\text{theory})
\end{aligned} \tag{3.2}$$

The central values for the proton were given in Ref. [10] and cited, with an estimation of uncertainties supplied by the current authors, in Refs. [17, 43]².

A justification of the theoretical uncertainties in eqs. (3.1) and (3.2), which are derived from order-by-order convergence of the results, will be the subject of the next two subsections. Here, we only remark that they encompass 68% intervals but that the corresponding probability is not distributed in a Gaussian manner. Note also that the statistical error from fitting $\gamma_{M1M1}^{(p)}$ along with $\alpha_{E1}^{(p)}$ and $\beta_{M1}^{(p)}$ in Ref. [10] is inherited by related quantities, including $\gamma_{M1M1}^{(n)}$; cf. Sect. 2.2.2.

Figure 4 illustrates the pattern of convergence and the 1σ ellipses for the scalar polarisabilities. At present, there is only a weak signal that proton and neutron polarisabilities differ, and then only if the Baldin sum rule is used. The ellipses are obtained by adding all uncertainties (statistical, Baldin, and truncation) in quadrature. The truncation error plays a minor role, so although, strictly speaking, its non-Gaussian distribution (see Sect. 3.2 below) mandates a more sophisticated treatment of error combination, that would not lead to ellipses which are appreciably different from those shown here.

Table 1 gives the comparison with the recent MAMI extraction of the proton spin polarisabilities from the first double-polarised Compton measurements [17]. These extractions were constrained to reproduce the listed values of two linear combinations, namely the forward and backward spin polarisabilities γ_0 [53, 54, 58] and γ_π [55]. (Note, however, that the value for γ_0 is much more model-independent than that for γ_π .) Within their stated uncertainties, they all overlap our 68% confidence intervals. This agreement, and specifically the agreement for $\gamma_{M1M1}^{(p)}$, supports our previously-developed strategy of promoting and fitting the isoscalar LEC of γ_{M1M1} to unpolarised data [10]. Future experiments on double-polarisation observables on the proton and light nuclei that are running or approved at MAMI and HI γ S will provide high-accuracy data for more conclusive comparisons [12–15]. A χ EFT analysis of the polarised scattering data for the proton is forthcoming [38].

²The errors of $\{\pm 1.8; \pm 0.7; \pm 0.4; \pm 0.4\}$ cited in Refs. [17, 43], though supplied by us, differ slightly from these. That is because eq. (3.2) reflects the difference in power-counting for amplitudes and polarisabilities discussed in Sect. 2.2; considers isoscalar and isovector convergence separately; and uses the Bayesian framework described below to calculate 68% intervals from the EFT truncation error. With the possible exception of γ_{E1M2} , we do not consider the change in uncertainties significant—cf. the discussion below of how well uncertainties can be estimated.

| | this work: $\mathcal{O}(e^2\delta^{-2})$ | NLO B χ PT | MAMI | DR(I) | DR(II) |
|-----------------------|--|-----------------|------------------------|--------|--------|
| $\gamma_{E1E1}^{(p)}$ | -1.1 ± 1.9 | -3.3 ± 0.8 | -3.5 ± 1.2 | -3.4 | -4.3 |
| $\gamma_{M1M1}^{(p)}$ | $2.2 \pm 0.5(\text{stat}) \pm 0.6$ | 2.9 ± 1.5 | 3.2 ± 0.9 | 2.7 | 2.9 |
| $\gamma_{E1M2}^{(p)}$ | -0.4 ± 0.6 | 0.2 ± 0.2 | -0.7 ± 1.2 | 0.3 | 0.0 |
| $\gamma_{M1E2}^{(p)}$ | 1.9 ± 0.5 | 1.1 ± 0.3 | 2.0 ± 0.3 | 1.9 | 2.2 |
| $\gamma_0^{(p)}$ | $-2.6 \pm 0.5(\text{stat}) \pm 1.8$ | -0.9 ± 1.4 | $-1.0 \pm 0.1 \pm 0.1$ | -1.5 | -0.8 |
| $\gamma_\pi^{(p)}$ | $5.5 \pm 0.5(\text{stat}) \pm 1.8$ | 7.2 ± 1.7 | 8.0 ± 1.8 | 7.8 | 9.4 |

Table 1: Values of the proton spin polarisabilities from the current calculation, from covariant χ PT at NLO [52], from experiment (“MAMI” [17]; incorporating γ_0 : [53, 54] and γ_π : [55]); and from Dispersion Relations (I) [42], (II) [9, 17, 56, 57].

At this order, the only differences between neutron and proton spin polarisabilities come from the pion-cloud corrections of eq. (2.9). Little is known about the neutron spin polarisabilities. Our prediction $\gamma_0^{(n)} = 0.5 \pm 0.5(\text{stat}) \pm 1.8$ is certainly compatible with the expectation that this quantity should be “about zero” [59]. For $\gamma_\pi^{(n)}$, our value is $7.7 \pm 0.5(\text{stat}) \pm 1.8$. This places us on the low end of the range 12.7 ± 4.0 extracted in a DR framework from the reaction $\gamma d \rightarrow \gamma pn$ [60], but uncertainties in that theory may be underestimated [1].

3.2 A Theory Of Theoretical Uncertainties

The intrinsic uncertainty of any EFT calculation comes from the truncation of the EFT series at a finite order k . It is clear that definitive results for terms in the series that have not been computed are impossible to obtain. Nevertheless, estimates of the EFT truncation error can be made using the same strategy as in other perturbative quantum field theories, i.e., by combining knowledge of the perturbative parameter with reasonable assumptions about the behavior of higher-order coefficients. Ref. [39] used Bayesian methods to implement this strategy for perturbative QCD, and Ref. [40] adapted the approach to EFTs. Other methods for estimating the truncation error are certainly possible, but this Bayesian framework has the advantage that it allows clear specification of premises: it facilitates a rigorous derivation of the theoretical uncertainties from a particular assumption about the behaviour of higher-order coefficients in the EFT series. Note that we work in the leading-omitted-term approximation, i.e. we assume the error associated with that term dominates the theoretical uncertainty. As long as χ EFT is convergent, this is a reasonable assumption (cf. discussion of its accuracy below). We also point out that Bayesian methods can aid in the extraction and uncertainty estimation of χ EFT LECs that appear in the nucleon polarisabilities [61, 62], but we do not pursue that avenue here, instead applying them only to truncation errors.

Suppose we have computed k non-trivial orders of a generic polarisability ξ , with the

first (leading) order being c_0 :

$$\xi_{(k)} = \sum_{n=0}^{k-1} c_n \delta^n . \quad (3.3)$$

The canonical EFT estimate of the truncation error, R_ξ , is then determined by the largest magnitude of the coefficients c_n as follows:

$$R_\xi = \max_n \{|c_n| : n = 0, \dots, k-1\} \times \delta^k . \quad (3.4)$$

Equation (3.4) was the basis of the determination of the truncation error of scalar polarisabilities in Refs. [1, 10]. An entirely equivalent error estimation was recently articulated and advocated for two- and three-nucleon-system observables in Refs. [63–65].

We want to understand how to interpret such a truncation error. To do that, we compute the probability distribution function (pdf), denoted $\text{pr}(\Delta|I)$, namely the degree of belief that a polarisability will take a specific value which differs by an amount Δ from the calculated central value $\xi_{(k)}$ of the χ EFT prediction at order k . This belief is based upon the available information I which includes the order k of the calculation, the behaviour of the χ EFT series, our expectations regarding naturalness, and—in the case of fitted polarisabilities—data at the physical pion mass. There is no reason to assume this pdf will be Gaussian; in general, it is not. Nevertheless, it can still be integrated to compute degree-of-belief intervals (DoB intervals), such as the Bayesian analogue of the usual 68% (1σ) and 95% (2σ) confidence intervals.

Since this is a Bayesian approach, a choice of prior for the coefficients c_j associated with the higher-order terms is mandatory. We implement a prior which assigns uniform probability to any value of the omitted coefficients, up to some unspecified maximum, as for prior $A_\epsilon^{(1)}$ of Ref. [40]. These assumptions lead to analytic expressions for the probability distribution:

$$\text{pr}(\Delta|R_\xi, k) = \frac{k}{k+1} \frac{1}{2R_\xi} \times \begin{cases} 1 & \text{for } |\Delta| \leq R_\xi \\ \left(\frac{R_\xi}{|\Delta|}\right)^{k+1} & \text{for } |\Delta| > R_\xi \end{cases} \quad (3.5)$$

For $k = 1, 2, 3$, these pdfs are illustrated for in Fig. 5. By integration of the pdf, we define σ_ξ such that $[\xi_{(k)} - \sigma_\xi; \xi_{(k)} + \sigma_\xi]$ is the 68% DoB interval. This is also how we define the theoretical or truncation error in eqs. (3.1) and (3.2), and throughout this work. For comparison, the standard EFT error estimate, $[\xi_{(k)} - R_\xi; \xi_{(k)} + R_\xi]$, is a $\frac{k}{k+1} \times 100\%$ DoB interval. For two of the cases we are concerned with, namely $k = 2$ and $k = 3$, these are 67% and 75% intervals, respectively, so there is little difference between R_ξ and σ_ξ .

We close with a few comments. First, the truncation uncertainty (3.5) is not distributed in a Gaussian way. This can be understood as follows. Each time a new order is calculated, more information is gleaned about the largest-possible coefficient in the series. That the probability is equidistributed for any value inside the standard EFT interval between zero and R_ξ is inherited from our choice of prior. On the other hand, the probability of finding a coefficient larger than the maximum of those obtained thus far becomes smaller the more

orders are known—a fact represented by the steeper power-law falloff above the maximum as the EFT calculation’s order increases. Indeed, the 95% DoB interval of the pdf in eq. (3.5) is not twice as large as the 68% interval σ_ξ , as would be expected for a Gaussian pdf; see also the examples in Fig. 5 below. Instead, it lies at about 7σ for $k = 1$, 2.6σ for $k = 2$, and 1.9σ for $k = 3$. Second, in cases where we know that one of the c_n is *a priori* zero, e.g. by symmetry arguments, since the power-law falloff of the pdf outside the “standard” EFT interval is determined by the number of non-trivial orders computed, the value of k to be used in eq. (3.5) must then be reduced by one.

Different interpretations of the naturalness of EFT coefficients are encoded in different priors, and those in turn can produce somewhat different 68% DoB intervals. In Ref. [40], several possibilities for the naturalness prior were considered and it was demonstrated that—once three orders in the EFT series are known—those different interpretations of naturalness led to a 10–15% variation in the truncation error. However, the variation is larger if fewer coefficients in the series have been computed, as then the specific form of the prior plays more of a role in determining the final error. Furthermore, our invocation of the first-omitted-term approximation means that our error bands have a fractional uncertainty that could be as large as $\mathcal{O}(\delta)$, although the actual impact of terms beyond the (first omitted) δ^k term of Eq. (3.4) depends on whether coefficients at order k and beyond are correlated, uncorrelated, or anti-correlated [40]. Regardless, this suggests that the truncation error computed here should be understood to itself have an accuracy of $\pm 20\%$. The errors quoted below should be read with this in mind. For uniformity of presentation, we quote all errors to one decimal place, but in certain instances this may constitute spurious precision.

3.3 Assigning Theoretical Uncertainties to Spin Polarisabilities

The values of the spin polarisabilities at $\mathcal{O}(e^2\delta^{-4})$ and $\mathcal{O}(e^2\delta^{-2})$ are given in Table 2. The first order is isoscalar, while the next one contains both isoscalar and isovector components. The series for the isoscalar spin polarisabilities is therefore computed to an accuracy of $k = 2$ nonzero orders; the contribution of order δ^1 relative to LO is zero, and so we know only c_0 and c_2 in eq. (3.4). We hence obtain the results for the isoscalar remainder R_ξ from eq. (3.4) shown in Table 2. In practice c_2 is the larger coefficient in each case, and so R_{γ_i} is δ times the $e^2\delta^{-2}$ contribution. Comparing with eq. (3.5) for $k = 2$, we find that this remainder can be interpreted as a 67% DoB interval. For the isovector spin polarisabilities we only have one order, and so R_{γ_i} is δ times the total and the corresponding DoB interval is only 50%.

To get the pdf of the truncation error for an individual nucleon, we convolute the two pdfs:

$$\text{pr}_\xi(\Delta) \equiv \text{pr}(\Delta | R_\xi^{(s)}, k^{(s)}, R_\xi^{(v)}, k^{(v)}) = \int_{-\infty}^{\infty} dy \text{pr}(y | R_\xi^{(s)}, k^{(s)}) \text{pr}(\Delta - y | R_\xi^{(v)}, k^{(v)}) \quad , \quad (3.6)$$

with obvious notation for isovector and isoscalar pieces. As Fig. 5 shows, this smears out the individual pdfs considerably so that they look somewhat more Gaussian. Results are the

| | γ_{E1E1} | γ_{M1M1} | γ_{E1M2} | γ_{M1E2} |
|----------------------------|-----------------|-----------------|-----------------|-----------------|
| isoscalar $e^2\delta^{-4}$ | -5.7 | -1.1 | 1.1 | 1.1 |
| isoscalar $e^2\delta^{-2}$ | -2.6 ± 1.3 | 1.8 ± 0.5 | -0.3 ± 0.6 | 2.2 ± 0.4 |
| isovector $e^2\delta^{-2}$ | 1.5 ± 0.6 | 0.5 ± 0.2 | -0.1 ± 0.1 | -0.2 ± 0.1 |

Table 2: Predictions of the spin polarisabilities at each χ EFT order. The total is given, so that the isoscalar *addition* at $\mathcal{O}(e^2\delta^{-2})$ is the difference between the first and second lines. At $\mathcal{O}(e^2\delta^{-2})$, the canonical EFT uncertainty estimates R_{γ_i} of eq. (3.4) is shown as an error on the central value (in this table only, this “error” is not the 68% DoB interval).

same for the proton and neutron. The additional convolution makes the relation between 95% and 68% DoBs depend on both $\Delta^{(s)}$ and $\Delta^{(v)}$.

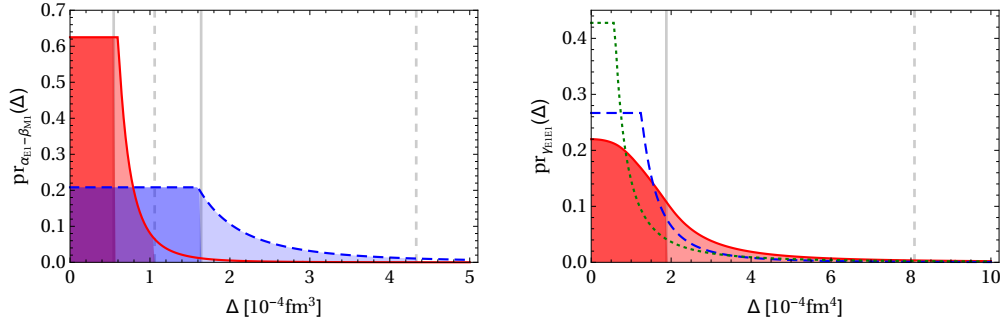


Figure 5: (Colour online) Examples of pdfs. Left: The pdf of $\alpha_{E1}-\beta_{M1}$ at the physical point for the proton (red solid) and neutron (blue dashed) as resulting from the fits underlying eq. (3.1), at N²LO for the proton ($k=3$, $R_{\alpha_{E1}-\beta_{M1}}=0.6$ in eq. (3.5)) and NLO for the neutron ($k=2$, $R_{\alpha_{E1}-\beta_{M1}}=1.6$). Right: The pdf of the truncation error in γ_{E1E1} at the physical point. The green dotted line shows the isovector combination’s truncation error ($k^{(v)}=1$, $R_{\gamma_{E1E1}}^{(v)}=0.6$), the blue dashed line that of the isoscalar ($k^{(s)}=2$, $R_{\gamma_{E1E1}}^{(s)}=1.3$), and the red line is the pdf that results from the integration in eq. (3.6). The solid (dashed) grey line denotes the 68% (95%) DoB interval. Pdfs for all polarisabilities are available in the Appendix.

In all cases, simply adding isoscalar and isovector errors linearly yields ranges that are near-identical to the 68% DoB intervals. One could also choose to study proton and neutron convergence patterns separately, instead of those of the isoscalar and isovector quantities. In general this produces somewhat smaller errors; it never gives larger ones. For example, the proton uncertainty of γ_{E1E1} would be about equally large, while that for the neutron would be quite a bit smaller (± 0.7). Whether one uses the proton-neutron or the isospin basis is a question of choice. We take the latter because its error assessments are more conservative and because χ EFT is most naturally formulated in the isospin basis.

We now turn to γ_{M1M1} since its expansion is more complicated. As mentioned above,

it is, strictly speaking, not a free parameter at the order to which we work, but in practice its proton value was obtained from a fit to unpolarised proton data. This requires the promotion of a LEC from the fifth-order πN Lagrangian. A further complication is that its Delta-pole contribution of $+2.8$, which is nominally suppressed by δ^2 , is more than twice the LO contribution. The contribution of $\pi\Delta$ loops is tiny. The origin of this, of course, is the large size of the magnetic $\gamma N\Delta$ coupling b_1 , whose square enters the leading pole contribution for γ_{M1M1} but not the other spin polarisabilities (see eq. (2.12)). As a result, the pole contribution is about 6 times as large as if b_1 were of natural size. There is precedent for promoting terms involving coefficients which are unnaturally large, see e.g. [66], and hence for γ_{M1M1} we treat the b_1^2 contribution to the Delta pole as suppressed by only one power of δ , giving $k = 3$ nontrivial orders in our expansion. The calculation is still complete to N²LO as any other graphs involving b_1^2 will be suppressed by δ^4 ; thus only the error estimate is affected by the reordering. With neither of these adjustments, we would predict the proton value to be 6.4 ± 3.0 , which is in fact still compatible with our quoted result of $2.2 \pm 0.5(\text{stat}) \pm 0.6(\text{theory})$. However several lines of evidence, though not conclusive, suggest the latter is a more appropriate central value and uncertainty; these include the close similarity of the values in the third and fourth-order extractions of the scalar polarisabilities discussed in Ref. [10], as well as the DR and MAMI values quoted in Table 1.

Finally, the forward and backward spin polarisabilities of eq. (2.4) are not independent of the multipole spin polarisabilities. Their errors could thus be assessed naively as ± 2.1 by adding the individual multipole errors in quadrature, if the individual errors were Gaussian distributed. Since both also inherit the large Delta-pole contribution as well as the fitted LEC from γ_{M1M1} , we instead assess their theoretical uncertainties by the same prescription as for γ_{M1M1} . As both are linear combinations of quantities which are sensitive to different multipolarities, and hence different physical mechanisms, *a priori* we expect the two errors to be similar. Surprisingly, we find an error of γ_π that is half that of γ_0 . We see no physical reason for this. Furthermore, when in Sect. 4.1, we look at values of m_π greater than the physical value, the difference between the γ_0 and γ_π errors disappears for $m_\pi \gtrsim 170$ MeV. This suggests that the rather small uncertainty for γ_π found via the order-by-order prescription at m_π^{phys} is accidental. Therefore, for all m_π , we will use as the error of γ_π that derived by Bayesian criteria for γ_0 . The resulting $\gamma_\pi^{(p)}$ uncertainty of ± 1.8 at m_π^{phys} is then close to the added-in-quadrature result.

We close with remarks which pertain to scalar polarisabilities; further discussion can be found in Sect. 4.1. Our previously-published uncertainties of eq. (3.1) were also obtained by considering order-by-order convergence, though without the rigorous framework provided here. For the proton, there are three non-vanishing orders ($k = 3$) and the uncertainties should be interpreted as the 75% DoB interval for the pdf, rather than 68% DoB intervals. For the neutron, though, $k = 2$ for the extracted scalar polarisabilities, so the DoB is 67%, but statistical uncertainties there far outweigh the theoretical accuracy. For either nucleon, our previous remainder estimates R_ξ and the new 68%-DoBs σ_ξ are identical after rounding. A determination for the neutron at $\mathcal{O}(e^2\delta^4)$ in the amplitudes is forthcoming [67]. Figure 5 shows the plots of the pdfs for $\alpha_{E1} - \beta_{M1}$, the one free variable after the Baldin sum rule is

used as a constraint.

3.4 Convergence Tests: Selected Higher-Order Terms

To check our error estimate at m_π^{phys} , we look at the effect of including selected, renormalisation-group-invariant, higher-order corrections. This does not lead to increased accuracy; in general that is only achieved when all contributions at a given order are known. It can, however, add credence to our procedure if contributions fall within the derived error estimates. Since Refs. [1, 10, 11] have already discussed various such effects for the scalar polarisabilities, we here consider only the spin polarisabilities.

As mentioned in Sect. 2.2, some contributions are known in variants which differ by contributions at $\mathcal{O}(\delta^3)$ relative to LO, i.e. at the first order not calculated. We will also use these variants to discuss the reliability of our uncertainty estimate of the m_π -dependence in Sect. 4.1.

- (1) Vertex corrections to b_1 and b_2 are reported in Ref. [10]. They add 0.1 units to γ_{E1E1} and γ_{E1M2} , -0.37 to γ_{M1M1} , and -0.2 to γ_{M1E2} , well within our proposed theoretical uncertainties.
- (2) The $\pi\Delta$ contributions in the heavy-baryon version of eqs. (2.13) and (2.14) differ by terms of $\mathcal{O}(e^2\delta^{-1})$ from a covariant version [52]. The latter add -0.2 to γ_{E1E1} , -0.4 to γ_{M1M1} , 0.3 to γ_{E1M2} and 0.03 to γ_{M1E2} , again in accord with our error bars.
- (3) The difference between the covariant Delta-pole result of eqs. (2.11) and (2.12) and the heavy-baryon one enters at $\mathcal{O}(e^2\delta^{-1})$ as well. The latter sets the $E2$ -coupling b_2 and recoil effects to zero and uses a different value of $b_1^{\text{HB}} \approx 4.8$ [1, 10]. We find the heavy-baryon version adds 0.35 units to γ_{E1E1} , 0.8 to γ_{M1M1} , 0.4 to γ_{E1M2} and -0.3 to γ_{M1E2} . These are within the quoted uncertainties.

In each case, the changes quoted for γ_{M1M1} do not take into account the fact that it needs to be refitted once such effects are added; we expect this to decrease the magnitude of higher-order effects.

4 Chiral Extrapolations

A chiral extrapolation of the central values for the polarisabilities simply uses the pion-mass dependence of the χEFT results in Sect. 2.2 to generate the functions $\xi(m_\pi)$. The final results are shown as solid red (proton) and blue (neutron) lines in all the plots of Sect. 4.3.

Just as at the physical point, the chiral predictions have truncation errors which are assessed as before, but now are functions of m_π ; we will make a few technical remarks on their evaluation in Sect. 4.1. The truncation uncertainties are represented in the plots by shaded bands for as far as we trust them; see Sect. 4.2. These error bands at unphysical pion masses correspond only to the “theory” error. The full error is then obtained by combining this with the (m_π -independent) statistical and (for scalar polarisabilities) Baldin-sum-rule

errors. Therefore, in the plots, we mark the total error only at the physical point, adding all errors linearly. In cases where the physical-point error is larger than the width of the band, the whole band can be moved up or down within this difference; see details in Sect. 4.3. This presentation has been chosen to highlight the running of the error with the pion mass, and because the other sources of error depend on the current state of the data, and thus may change in future. The different sources of errors could of course be combined in a Bayesian formalism, but that is outside the scope of this paper.

Finally, we do not consider any implicit m_π -dependence of g_A , f_π , M_N , Δ_M , c_i , etc. All such effects are of higher order in the chiral counting. For example, the correction to $g_A(m_\pi) = g_A^0 + \mathcal{O}(m_\pi^2)$ [68] is suppressed by two orders in m_π/Λ_χ and hence beyond the accuracy of our results.

4.1 Theoretical Uncertainties near the Physical Point

We first consider the uncertainties in regime (i), $m_\pi \approx m_\pi^{\text{phys}}$. There, we have included those contributions to the polarisabilities that are required in the physical low-energy Compton amplitudes up to $\mathcal{O}(e^2\delta^4)$. Omitted terms are therefore $\mathcal{O}(\delta^3)$ relative to leading. Ignoring a few details to be discussed shortly, we estimate the remainder $R_\xi(m_\pi)$ and 68% DoBs $\sigma_\xi(m_\pi)$ at any given m_π in regime (i) just as we did at m_π^{phys} in Sect. 3.3.

The only difference is in the expansion parameter δ , which was defined in Sect. 2 and enters in eqs. (3.3) and (3.4). So long as we remain well below $m_\pi \approx \Delta_M$, it could be taken to be constant, $\delta \approx 0.4$. But, in practice, some chiral corrections to pion loops grow linearly with m_π , and once $m_\pi \approx \Delta_M$ the whole counting changes: Delta graphs become as important as nucleon ones; see Sect. 2.1 and the next subsection. Hence, we choose a value of δ which increases with m_π ,

$$\delta(m_\pi) = 0.4 \frac{m_\pi}{m_\pi^{\text{phys}}} . \quad (4.1)$$

For the three spin polarisabilities which are pure predictions, γ_{E1E1} , γ_{E1M2} and γ_{M1E2} , there is little more to be said. As at the physical point, at any given m_π we derive the isoscalar and isovector uncertainties from the order-by-order convergence of their respective series, and obtain the total uncertainty by convoluting the corresponding pdfs. The overall scale of their isoscalar uncertainty $R_{\gamma_i}^{(s)}$ turns out to be dominated by δ times the $\mathcal{O}(e^2\delta^{-2})$ contribution at all pion masses we consider. In each case, the absolute error increases rather modestly as a function of m_π , mainly because an important part of the $\mathcal{O}(e^2\delta^{-2})$ contribution is actually falling as $1/m_\pi$ while the expansion parameter $\delta(m_\pi)$ grows linearly. The ordering of contributions to γ_{M1M1} , γ_0 and γ_π for $m_\pi \neq m_\pi^{\text{phys}}$ also mirrors exactly that at the physical point as discussed in Sect. 3.3: terms quadratic in the rather large coupling b_1^2 are promoted by one order.

The scalar polarisabilities require a little more discussion, since we did not derive in detail their errors at the physical point, these having been determined through fits to data [10, 11]. First, we recall that the fit of $\alpha_{E1}^{(n)}$ and $\beta_{M1}^{(n)}$ to deuteron data used amplitudes only at NLO, while that for the proton used those at one order higher. This leads to substantially larger truncation errors at the physical point than that for the proton: ± 0.8 as opposed

to ± 0.3 . However, their running with m_π is predicted in χ EFT to N²LO for both. Thus, when generating the scalar-polarisability error bands in the neutron case, we use the same uncertainties as for the proton, while including the larger truncation uncertainty in the error bar at the physical point. Once again, any change in the central value of $\alpha_{E1}^{(n)}$ and $\beta_{M1}^{(n)}$ resulting from a new fit to deuteron data at order δ^2 rather than δ^1 relative to LO only serves to move the curve up and down. A construction of isoscalar and isovector uncertainties as for the spin-polarisabilities, with reasonable assumptions as to how much $\alpha_{E1}^{(n)} - \beta_{M1}^{(n)}$ may shift in an future N²LO fit, produces near-identical bands.

Furthermore, in the proton fits of Ref. [10], the actual fit parameter was $\alpha_{E1}^{(p)} - \beta_{M1}^{(p)}$, with $\alpha_{E1}^{(p)} + \beta_{M1}^{(p)}$ fixed by the Baldin sum rule. The scale R of the uncertainty was obtained by considering $\alpha_{E1}^{(p)} - \beta_{M1}^{(p)}$ as *predicted* at LO— $\mathcal{O}(e^2\delta^{-2})$ —and *fit* at the next two orders. By fitting the amplitudes at NLO, the LECs $\alpha_{E1}^{(p)\text{LEC}}$ and $\beta_{M1}^{(p)\text{LEC}}$ are promoted by one order. In practice, the proton fits at orders δ^1 and δ^2 relative to LO gave almost identical values for $\alpha_{E1}^{(p)\text{LEC}} - \beta_{M1}^{(p)\text{LEC}}$. To reflect this, we treat the LECs as part of the $\mathcal{O}(e^2\delta^{-1})$ contribution to $\alpha_{E1}^{(p)}$ and $\beta_{M1}^{(p)}$. The additional contribution at $\mathcal{O}(e^2\delta^0)$ is then subtracted to give zero at the physical point, and so affects $\alpha_{E1}^{(p)} - \beta_{M1}^{(p)}$ only for $m_\pi \neq m_\pi^{\text{phys}}$.

Beyond the physical point, we continue to treat $\alpha_{E1} + \beta_{M1}$ and $\alpha_{E1} - \beta_{M1}$ as independent. However, the Baldin sum rule for $\alpha_{E1} + \beta_{M1}$ is special: at the physical point it provides extrinsic information in our NLO and N²LO fits and should be reproduced exactly. In fact, higher-order effects in the scalar-polarisability sum for the proton at the physical point are tiny compared to the LO prediction of 13.9 from eq. (2.5). We therefore base our error estimates for $\alpha_{E1}^{(p)} + \beta_{M1}^{(p)}$ beyond the physical point only on the shifts from the LO term, i.e. we drop c_0 in the construction of R_ξ in eq. (3.4); we then have $k = 2$ for $\alpha_{E1}^{(p)} + \beta_{M1}^{(p)}$. We considered several variants of this procedure, but they do not substantially alter the outcome: while the χ EFT uncertainty at m_π^{phys} is indeed zero, it grows very rapidly with m_π , see Fig. 8. A several-hundred-per-cent error at $m_\pi = 350$ MeV, while technically correct for a theory defined as an expansion around the chiral limit, seems overly pessimistic. Indeed, it defies the quite conservative expectation that $\alpha_{E1} + \beta_{M1}$ tends asymptotically to a constant as m_π gets bigger, since the nucleon size, and hence the typical size over which its charged constituents can fluctuate, will not increase with m_π . The χ EFT error evolution for $\alpha_{E1}^{(p)} - \beta_{M1}^{(p)}$ is more modest, and is more representative of the truncation error in χ EFT predictions for polarisabilities. Well away from the physical point and the constraint provided by the Baldin sum rule, there is no particular logic to using $\alpha_{E1} \pm \beta_{M1}$, rather than α_{E1} and β_{M1} separately, as the quantities via which we assess convergence of the χ EFT series. Once m_π reaches 250 MeV, α_{E1} and β_{M1} separately have much better convergence properties than does $\alpha_{E1} + \beta_{M1}$. For pion masses in that vicinity, taking the error only from $\alpha_{E1} - \beta_{M1}$ gives errors consistent with those obtained from analysing α_{E1} and β_{M1} separately. So, in what follows, we simply, if somewhat arbitrarily, assign zero truncation uncertainty for the evolution of $\alpha_{E1} + \beta_{M1}$ in order to generate our final results for α_{E1} and β_{M1} .

We then use different colours for the bands in the plot of $\alpha_{E1} + \beta_{M1}$ in Fig. 8 to indicate that they are not used to derive corridors for α_{E1} or β_{M1} . The widths of the corridors of the

scalar polarisabilities are set by half the uncertainty in $\alpha_{E1} - \beta_{M1}$, and their corridors are anti-correlated. The Baldin-related error is indicated, along with the statistical one, only at the physical point.

Figure 6 shows the evolution of the error bands for all six polarisabilities, but *not* the evolution of central values with m_π , the more clearly to display the behaviour of the uncertainties. As corroborating evidence for this error assessment, we proceed as in Sect. 3.4 to take advantage of the fact that three classes of (isoscalar) pion-mass-dependent higher-order corrections are known. However, only the first two display m_π -dependence: vertex corrections (blue dashed line) [10], and the inclusion of (some) $1/M_N$ corrections in $\pi\Delta$ loops via a covariant calculation (red dot-dashed line) [52]. Both effects are much smaller than our 68% uncertainty bands for all 6 polarisabilities, even in regime (ii), providing a potential hint that the errors may be over-estimated. We can safely conclude that our analysis of uncertainties passes reasonable checks both at the physical point (Sect. 3.1) and in regard to the m_π dependence.

4.2 Theoretical Uncertainties Well Beyond the Physical Pion Mass

For lattice calculations with m_π markedly larger than m_π^{phys} the regime (i) power counting employed in Sect. 4.1 is no longer appropriate, as discussed in Sect. 2.1. For $m_\pi \sim \Delta_M$ the scales $P(m_\pi)$ and ϵ of eq. (2.1) are of the same order, so there is no suppression of graphs according to the numbers of Delta propagators in them. Leading πN and $\pi\Delta$ loops and Delta-pole graphs are all on the same footing, contributing to the scalar polarisabilities at $\mathcal{O}(e^2\epsilon^{-1})$ and to the spin polarisabilities at $\mathcal{O}(e^2\epsilon^{-2})$. The subleading πN loops included above are suppressed by one power of ϵ but do not constitute a complete set of contributions at this order. There are, for instance, Delta-pole graphs with πN and $\pi\Delta$ loop corrections to the magnetic and electric $\gamma N\Delta$ vertices, and graphs like those of Fig. 2 with intermediate Delta propagators replacing one or more nucleon propagators. Some, but not all, of the latter are included in a covariant calculation [52]. Thus, in regime (ii) our calculation is only complete at leading order; there are omitted effects already at relative order ϵ .

Though we have not shown the results here, we did carry out a regime-(ii) error analysis. We found that for $m_\pi \sim \Delta_M$ the bands we generated were in broad agreement with the regime-(i) bands continued into this region. This is unsurprising in view of the fact that regime (i) and regime (ii) are not clearly separated; transition from one to the other is gradual.

In any case, it seems that χEFT does not adequately describe the behaviour of many observables seen in lattice computations for larger values of m_π [69–71]. For example, computations show the nucleon mass rising linearly with m_π beyond 300 MeV, not displaying the more complex dependence involving higher powers predicted by χEFT [72, 73]. Similar difficulties for χEFT are seen in other observables, too [74, 75].

Given these issues, we will show predictions for χEFT in regime (ii), but allow the regime-(i) error bars to fade away beyond $m_\pi \approx 250$ MeV, i.e. as they become unreliable, and disappear altogether beyond about 350 MeV. At such pion masses, linear extrapolations in m_π —as used in Refs. [73, 75] and earlier studies—may describe lattice QCD results, but

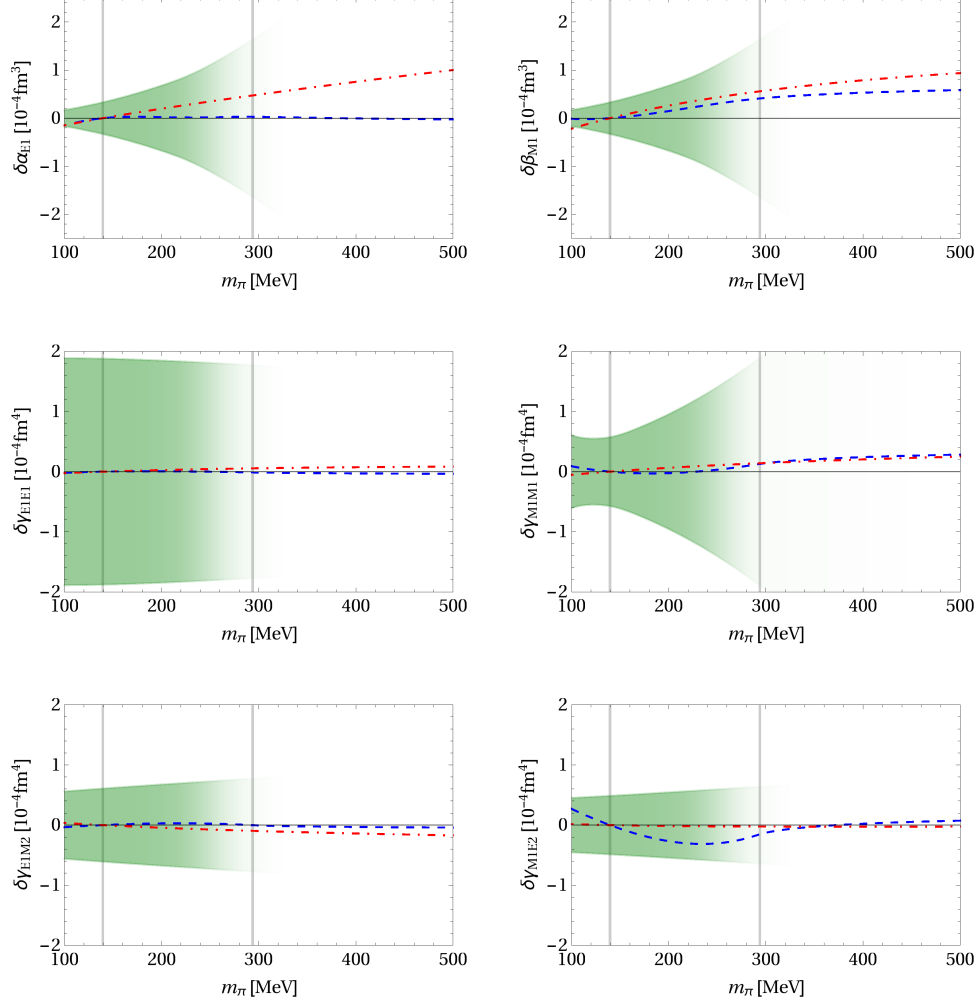


Figure 6: (Colour online) Error bands on theoretical results for m_π -dependence of polarisabilities. For greater clarity, the m_π -evolution of the central value is not shown. The lines demonstrate the added effect of selected next-order corrections to the m_π -dependence of the polarisabilities, normalised to zero at m_π^{phys} . Blue dashed: $\gamma N \Delta$ vertex corrections [10]; red dot-dashed: a set of “relativistic” corrections to $\pi \Delta$ amplitudes [52].

they are not justified within χEFT , and are more-or-less uncontrolled. We thus refer to results in this regime not as “chiral predictions” but as “chiral curves” and speculate as to why such extrapolations may be successful at the end of Sect. 5.

4.3 Results: Pion-Mass Dependence of Polarisabilities

The solid lines in Figs. 7 and 8 are χEFT predictions for the pion-mass dependence of the dipole polarisabilities, together with their theoretical uncertainties, computed as specified

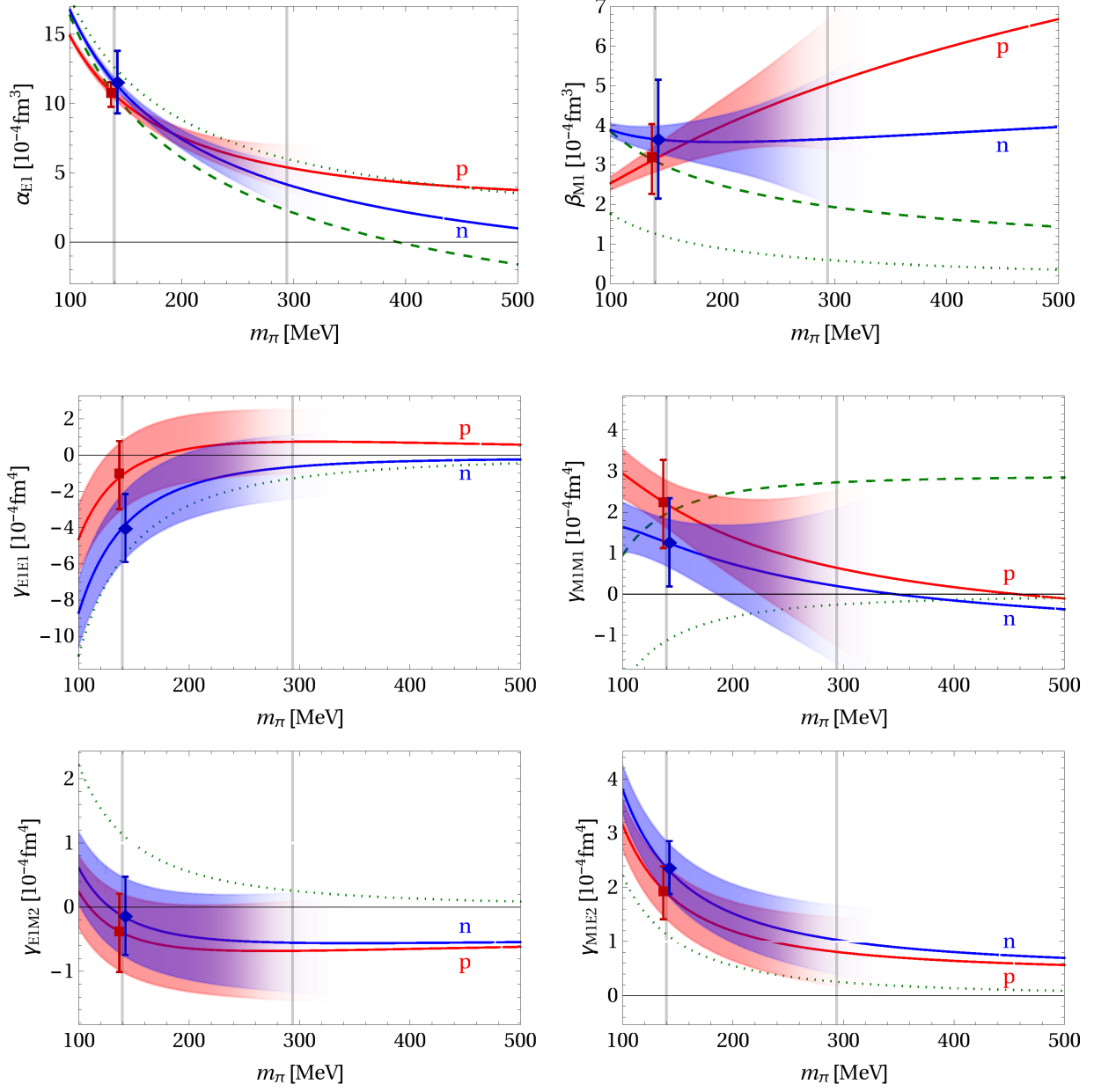


Figure 7: (Colour online) Predicted m_π -dependence of the dipole polarisabilities in χ EFT. The full result is represented by solid lines and labelled for the respective nucleon: proton results are coloured red with red corridors of χ EFT uncertainties and symbol \blacksquare at m_π^{phys} (slightly offset to smaller m_π for better visibility); neutron results are blue with blue corridors and \blacklozenge at m_π^{phys} (slightly offset to larger m_π). Error bars at the physical point add statistical, theory and Baldin-sum-rule errors linearly, as applicable. Green lines are isoscalar, with dotted: leading π N contributions; dashed (for α_{E1} , β_{M1} and γ_{M1M1} only): Delta pole and leading $\pi\Delta$ pieces added, plus isoscalar LECs for α_{E1} , β_{M1} . The vertical lines show the position of the physical pion mass and the Delta-nucleon mass difference. See text for additional details.

in Sects. 4.1 and 4.2. These are complete at order δ^2 relative to LO for all polarisabilities, and include three nonzero orders for α_{E1} , β_{M1} , γ_{M1M1} , γ_0 and γ_π , and two nonzero orders for the other polarisabilities. Proton results are colour-coded in red, neutron ones in blue, and isoscalar ones in green. The leading πN loops (green dotted) constitute LO in regime (i). The green dashed curves represent the complete isoscalar result at order δ^1 relative to LO in regime (i), as detailed in Sect. 3.3 and eq. (3.1). No new contribution arises at this order for γ_{E1E1} , γ_{E1M2} and γ_{M1E2} , and so this curve is absent there. In regime (ii), the solid and dashed curves are both only complete to LO, while the dotted curve is not even the full LO isovector result.

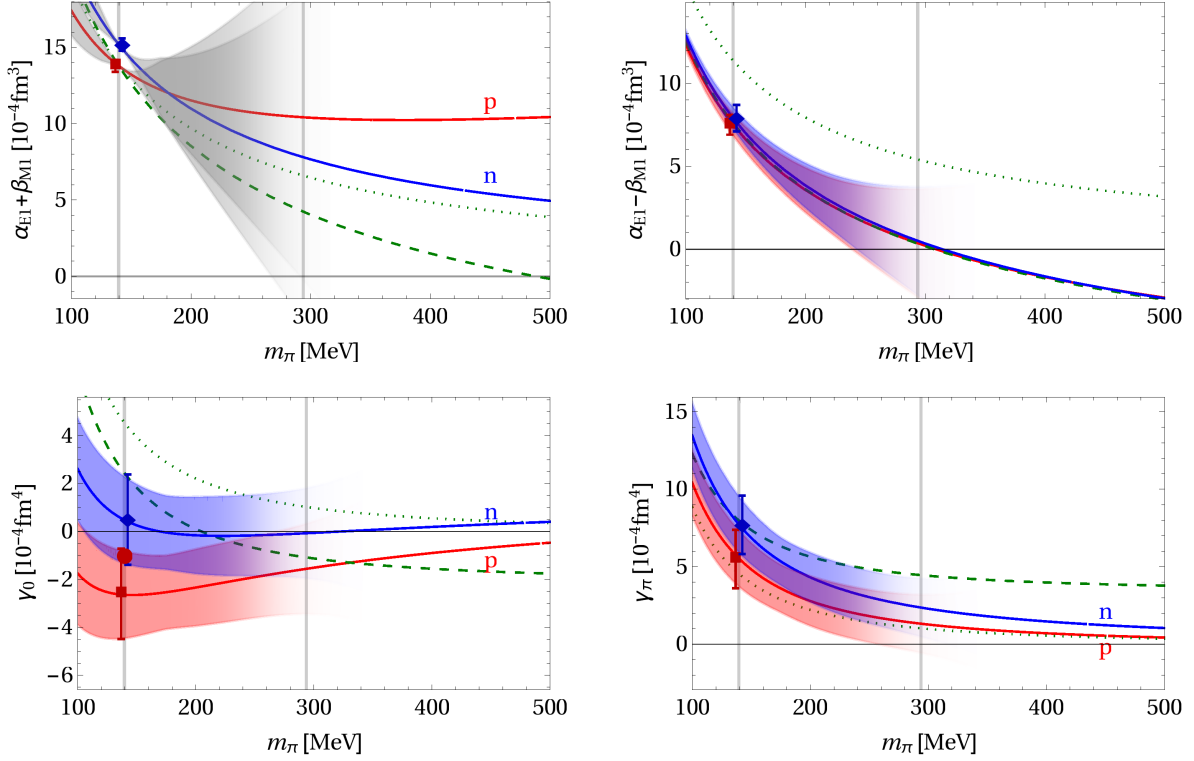


Figure 8: (Colour online) Pion-mass dependence of the Baldin sum rule (top left), $\alpha_{E1} - \beta_{M1}$ (top right), γ_0 (bottom left) and γ_π (bottom right). For $\alpha_{E1} + \beta_{M1}$, error bars at m_π^{phys} only reflect the uncertainties of the Baldin sum rules [47, 48]; in χEFT , such errors are input and are separate from the intrinsic χEFT errors. The χEFT uncertainty corridors of $\alpha_{E1} + \beta_{M1}$ are coloured differently to indicate that they are not used to derive corridors for α_{E1} or β_{M1} . The experimental value of $\gamma_0^{(p)}$ is indicated by the symbol \bullet [53, 54]; this result's uncertainty is smaller than the size of the symbol. Colour coding as in Fig. 7. See text for further details.

The symbols at the physical point are the χEFT predictions or, for α_{E1} , β_{M1} and γ_{M1M1} ,

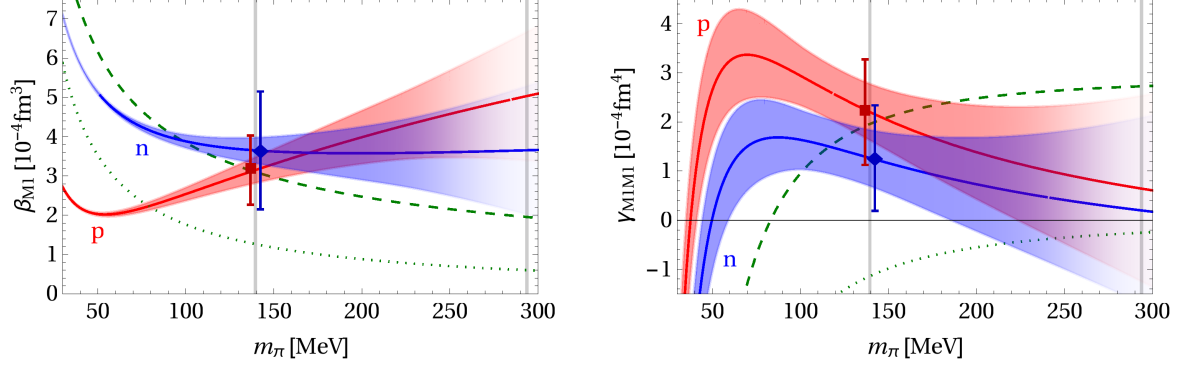


Figure 9: (Colour online) Pion-mass dependence of β_{M1} and γ_{M1M1} in regime (i). Legend as in Fig. 7.

fits. Their error bars are found by adding the theory and—where applicable—statistical plus Baldin-sum-rule errors linearly, as discussed at the beginning of Sect. 4. When this total error exceeds the width of the band at the physical point, the entire band can be floated up or down within that difference.

We see that the higher-order graphs have only a modest effect on the running of $\alpha_{E1} - \beta_{M1}$, γ_{E1E1} , γ_{E1M2} and γ_{M1E2} with m_π , but a major effect in the case of γ_{M1M1} , β_{M1} , γ_0 , $\alpha_{E1} + \beta_{M1}$, and, to some degree, γ_π . In addition, $\alpha_{E1} - \beta_{M1}$ is almost purely isoscalar. At the physical point, this is a simple consequence of the fact that the fitted proton and neutron values are very similar, cf. eq. (3.1). Beyond that, its isovector component grows only logarithmically with m_π and with a small pre-factor; see eq. (2.8). As already noted, we find it impossible to assign credible errors to $\alpha_{E1} + \beta_{M1}$, because of its poor convergence. The error bands on α_{E1} and β_{M1} in Fig. 7 are therefore simply half those of $\alpha_{E1} - \beta_{M1}$, and are anti-correlated. The uncertainties in the scalar polarisabilities then appear quite small relative to their magnitudes in both regimes (i) and (ii), while the uncertainties of the spin polarisabilities are comparable to their sizes.

As can be seen in Fig 7, in most cases the sub-leading πN loops do not have a major effect on the trend of the polarisabilities. However for β_{M1} and γ_{M1M1} , shown in the chirally relevant m_π -range in Fig. 9, they change functions which are monotonically decreasing (resp. increasing) with m_π at low orders into ones that are increasing (resp. decreasing) at m_π^{phys} . Indeed, both these polarisabilities could be regarded as somewhat fine-tuned at the physical pion mass, at least compared to their value at an arbitrary $m_\pi < m_\pi^{\text{phys}}$. This is interesting in light of the well-known puzzle that the magnetic polarisability has a physical value which is much smaller than predicted by the strong paramagnetic effects of the Delta. That higher-order terms in the m_π/M_N expansion could change the lower-order trend in β_{M1} was pointed out in Ref. [76]. At m_π^{phys} , pion-loop effects cancel against Delta-pole excitations to render the magnetic polarisability much smaller than either, and produce $\beta_{M1}^{(p)} \approx \beta_{M1}^{(n)}$.

Below the physical point, the isovector $N\pi$ corrections of eqs. (2.8) and (2.9) gain increasing statistical significance, destroying this cancellation for both proton and neutron; $\beta_{M1}^{(n)}$ quickly approaches its “natural” size in this low- m_π region, but flattens out once $m_\pi > m_\pi^{\text{phys}}$, while $\beta_{M1}^{(p)}$ changes from a decreasing to an increasing function around $m_\pi = 50$ MeV, and after that has a trend that is dictated by the sub-leading (isovector) πN loops.

A similar pattern is observed in γ_{M1M1} , whose leading dependence with $1/m_\pi^2$ dictates a much more prominent “turn-over” for $m_\pi < m_\pi^{\text{phys}}$. In this case the isovector component is smaller than for β_{M1} , but it is still statistically significant. The fact that $\gamma_{M1M1}^{(p)}$ is somewhat smaller at the physical point than its generic size for $m_\pi < m_\pi^{\text{phys}}$ may be related to the necessity to use γ_{M1M1} as a parameter in our recent extraction of the proton’s scalar polarisabilities in χEFT , cf. Sect. 2.2.2, even though the corresponding LEC only enters one order higher [10].

These issues merit further study. For the shape and physical-point value of these quantities to be markedly affected by contributions of still higher order, our error corridors would have to underestimate those effects. Our examination of select higher-order effects in Sect. 4.1 showed no such problems. Lattice computations closer to the chiral limit would provide excellent tests, but are numerically quite challenging.

4.4 Isovector Magnetic Polarisability and the Anthropic Principle

Isovector contributions of sub-leading πN loops enter at order δ^2 relative to LO for all polarisabilities, and the LECs of the scalar polarisabilities at the same order have isovector parts as well; see eq. (2.10). One thus expects that $\alpha_{E1}^{(v)}$ and $\beta_{M1}^{(v)}$ are about 20% of $\alpha_{E1}^{(s)}$ and $\beta_{M1}^{(s)}$, respectively. (Recall that we define $\xi^{(s,v)} = \frac{1}{2}(\xi^{(p)} \pm \xi^{(n)})$.) However, eq. (3.1) implies that these isovector combinations are zero within present uncertainties at the physical pion mass. This may signal another instance of fine-tuning between loops and short-distance physics at the physical point.

This can be quantified via the variation of the isovector polarisabilities with m_π (or equivalently m_q). At this order, the fitted LECs are m_π -independent, so the relevant rate of change is determined completely by long-distance physics associated with the subleading πN loops of eq. (2.8):

$$\left. \frac{d\beta_{M1}^{(v)}}{d \ln m_q} \right|_{m_\pi^{\text{phys}}} = 0.65 \pm 0.4 \quad , \quad \left. \frac{d\alpha_{E1}^{(v)}}{d \ln m_q} \right|_{m_\pi^{\text{phys}}} = 0.7 \pm 0.4 \quad , \quad (4.2)$$

in 10^{-4} fm^3 , and with a Bayesian estimate of the truncation error. Therefore, both $\alpha_{E1}^{(v)}$ and $\beta_{M1}^{(v)}$ vary strongly away from m_π^{phys} . Indeed, we have already seen in Figs. 7 and 9 that the similarity of proton and neutron polarisabilities disappears for $m_\pi \neq m_\pi^{\text{phys}}$. While the isovector component of $\alpha_{E1} - \beta_{M1}$ remains small at all m_π (see Fig. 8), the degeneracy of $\beta_{M1}^{(p)}$ and $\beta_{M1}^{(n)}$ at the physical point does seem to be something of an accident. Lattice results at $m_\pi = 806$ MeV corroborate this for β_{M1} [18]; see Sect. 5 for further discussion.

The Cottingham Sum rule relates the Compton scattering amplitude to the electromagnetic part of the proton-neutron self-energy difference, $\delta M_N^{\text{em}} \equiv M_p^{\text{em}} - M_n^{\text{em}}$ [29–33],

leading us to speculate about a potential rationale for this apparent coincidence. Though the topic is not without controversy and there is some scale-dependence in assigning strong and electromagnetic self-energy differences, there is broad agreement that δM_N^{em} and $\beta_{M1}^{(v)}$ are connected, since the latter is related to the value of a component of the integrand in the Cottingham sum rule at $q^2 = 0$ [29, 31, 33]. The strength of this connection depends, though, on assumptions about the integrand, and is hotly debated at present.

According to the analysis of Ref. [29], at the physical point the principal contributions to δM_N^{em} are an elastic piece of $[0.77 \pm 0.03]$ MeV, and an inelastic piece which is dominated by a term proportional to $\beta_{M1}^{(v)}$:

$$\delta M_N^\beta(m_\pi) = -A \beta_{M1}^{(v)}(m_\pi) . \quad (4.3)$$

The size of A can be obtained from Ref. [29]’s value of $\delta M_N^\beta \approx 0.5$ MeV for $\beta_{M1}^{(v)} = -0.5$. Both the elastic and inelastic part of δM_N^{em} involve integrals over form factors, well-known for the elastic contribution and estimated for the inelastic one. Assuming the pertinent scale in these form factors is associated with non-chiral physics, the variation of δM_N^{em} with quark mass will come mainly from the magnetic moment in the elastic term, and from β_{M1} in the inelastic term. Lattice QCD shows, though, that nucleon magnetic moments are rather insensitive to the quark mass [77], so we are left with δM_N^β as the dominant source of variation of δM_N^{em} with quark mass.

If we assume A of eq. (4.3) is m_π independent, we can estimate the variation of δM_N^β as

$$\left. \frac{d\delta M_N^\beta(m_\pi)}{d \ln m_q} \right|_{m_\pi^{\text{phys}}} = -0.65 \text{ MeV} . \quad (4.4)$$

Here, we do not give uncertainties, since we cannot quantify them on some of the assumptions being made. This value is not negligible relative to the quark-mass variation in Ref. [78]: $\left. \frac{d\delta M_N^{\text{strong}}}{d \ln m_q} \right|_{m_\pi^{\text{phys}}} \approx -2.1$ MeV (obtained under the assumption that m_u/m_d remains constant). Of course, the slope of δM_N^β could be smaller than our estimate, or somehow cancelled by other effects in δM_N^{em} . But the estimate (4.4) makes it plausible that—contrary to what was assumed heretofore in many works, such as Ref. [78]—the variation of δM_N^{em} is not negligible in comparison to that of the strong part.

If δM_N^β does indeed produce the largest variation of δM_N^{em} with m_q , our estimate suggests that the quark-mass dependence of the proton-neutron mass splitting may be significantly enhanced—or indeed reduced for $\beta_{M1}^{(p)} > \beta_{M1}^{(n)}$, which is within today’s allowed range. As a consequence, the neutron life-time would then either be substantially shortened as m_π increases (if $\beta_{M1}^{(p)} < \beta_{M1}^{(n)}$), or as m_π decreases (if $\beta_{M1}^{(p)} > \beta_{M1}^{(n)}$). A neutron that is too short-lived to allow Big-Bang Nucleosynthesis to proceed to ${}^4\text{He}$ presumably makes carbon-based life impossible. This putative connection between a small $\beta_{M1}^{(v)}$ and the Anthropic Principle deserves additional investigation.

On a more prosaic level, the connection to δM_N^β was used by Thomas et al. to extract values for $\beta_{M1}^{(v)}$ from the RBC lattice results for the electromagnetic self-energy of the nucleon [79]. They deduced small negative values (between -0.5 and 0) at four pion masses

between 279 and 683 MeV [32]. Neither our results for $\beta_{M1}^{(v)}$ nor the lattice computations by NPLQCD support this finding [18]; see Sect. 5. We point out here that the analysis of Ref. [32] assumes that other contributions to δM_N^{em} are completely negligible. Comparisons of direct measurements of polarisabilities in lattice QCD with our analysis are more satisfying, and it is to these that we now turn.

5 Comparison with Lattice Computations

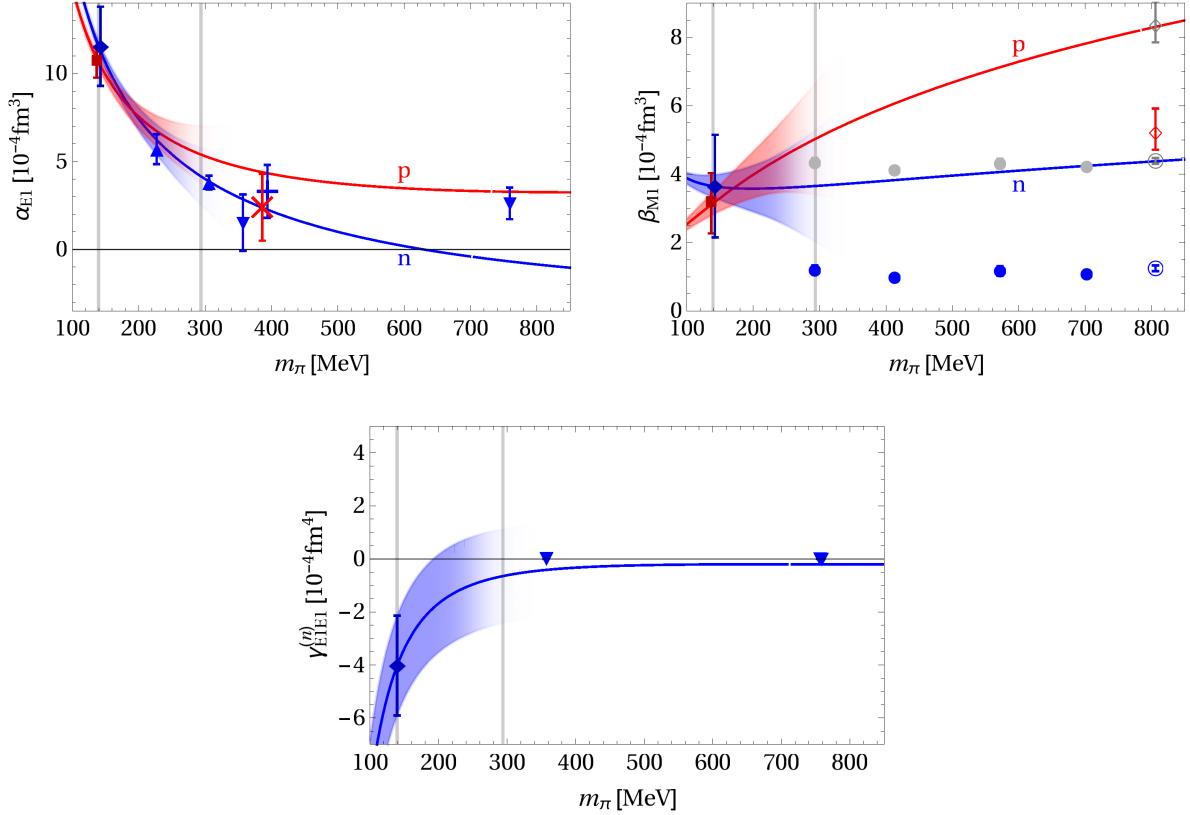


Figure 10: (Colour online) Comparison to lattice-QCD computations. Lattice computations of α_{E1} (top left): \blacktriangle (neutron) Lujan et al. [19]; \times (proton) and $+$ (neutron) Detmold et al. [20] (slight m_π -offset for better visibility); \blacktriangledown (neutron) Engelhardt/LHPC [24, 25]. Lattice computations of β_{M1} (top right): \bullet (neutron) Hall et al. [21, 22]; \diamond (proton) and \circ (neutron) NPLQCD [18]. Gray “ghost points” found by shifting all lattice results by $+3 \times 10^{-4} \text{ fm}^3$. Lattice computation of $\gamma_{E1E1}^{(n)}$ (bottom): \blacktriangledown (neutron) Engelhardt et al. [23, 26], see text for qualifier. For Refs. [21–23, 26], the reported lattice errors are smaller than our symbol sizes. Further notation as in Fig. 7, including \blacksquare for proton values and \blacklozenge for neutron ones at m_π^{phys} .

In Fig. 10, we compare our findings to emerging lattice-QCD computations of dipole polarisabilities. We do not report calculations without sea quarks—i.e. those that set the fermion determinant to one—and we have selected only references for pion masses up to about 850 MeV, with values that were either extrapolated to infinite volume and infinitesimal lattice spacing, or for which the authors estimated such effects to be irrelevant at present accuracies; cf. Refs. [80, 81]. To our knowledge, the work by Engelhardt/LHPC [24, 25] on $\alpha_{E1}^{(n)}$ is the only extant calculation which meets these criteria and also accounts for the charges of the sea quarks themselves. At present, all other computations use uncharged sea quarks whose mass is identical to that of the valence quarks. Several efforts to include charged sea-quark effects are ongoing [24, 25, 27]. We report lattice uncertainties as stated in the sources; a thorough appraisal of the lattice computations is not our goal. Note that an analysis of the consistency of lattice computations with our m_π -dependent predictions for polarisabilities cannot proceed by simple “standard-deviation counting”, because the uncertainties in the shape of $\xi(m_\pi)$, and thus also the theory errors at different pion masses, are highly correlated. Ref. [82] derives a modified χ^2 , whose use would be one way to account for such systematic errors.

We find that the χ EFT prediction for $\alpha_{E1}^{(n)}$ agrees well with the available computations, of Lujan et al. [19], Detmold et al. [20], and Engelhardt/LHPC [24, 25]. For the proton, only the result of Detmold et al. for α_{E1} at $m_\pi \approx 400$ MeV meets our selection criteria; it is quite compatible with the chiral curve. In regime (i) and (ii) these are statistically rigorous statements, since our error corridors provide estimates of higher-order effects—albeit with decreasing reliability as m_π increases. The agreement for electric polarisabilities is so good that we feel we must stress that our results are not fits to lattice computations; the physical value is determined by Compton-scattering data on the proton and deuteron, and the pion-mass dependence exclusively by chiral dynamics.

For the magnetic polarisability of the neutron, $\beta_{M1}^{(n)}$, we cannot reproduce the magnitude reported by the Adelaide group [21, 22]. NPLQCD [18] also reports results for $\beta_{M1}^{(n)}$ and $\beta_{M1}^{(p)}$ at 806 MeV; the former agrees well with the Adelaide results. The authors of this paper point out that, since this pion mass corresponds to the flavour SU(3) limit, their result for the isovector combination $\beta_{M1}^{(p)} - \beta_{M1}^{(n)}$ is unaffected by their neglect of sea-quark charges, in contradistinction to the isoscalar one. Interestingly, their isovector result agrees nearly exactly with the chiral curve. This is illustrated by the grey “ghost points” in the top right panel of Fig. 10, to which we have added constant isoscalar contribution of $3 \times 10^{-4} \text{ fm}^3$. This uncannily good agreement—at a pion mass of 800 MeV, which is certainly outside the radius of convergence of χ EFT—may of course be pure coincidence. Nevertheless, the lattice result of a sizeable isovector splitting at $m_\pi = 806$ MeV seems to support our finding in Sect. 4.4 that $\beta_{M1}^{(p)} \approx \beta_{M1}^{(n)}$ at the physical point is something of a coincidence. Lattice QCD calculations at intermediate pion masses will either strengthen or rebut this conclusion. They can also check if the χ EFT prediction of a significant $\alpha_{E1}^{(v)}$ for $m_\pi > m_\pi^{\text{phys}}$ is realised in QCD.

Engelhardt et al. have also reported the first lattice study of a spin polarisability [23, 26]. The neutron’s γ_{E1E1} shows a minuscule but nonzero signal within the reported uncertainties.

These values are without the subtraction of the pion-pole contribution in eq. (2.7). However, a calculation with uncharged sea quarks, like this one, has a number of pathologies. For example, in the two-flavour variant considered in Ref. [80], the isovector “pion-pole” contribution of the physical particle $\propto g_A \tau_3$ must be supplemented by a degenerate isoscalar-scalar ghost which couples with an unknown strength g_1 to the nucleon. If g_1 has a similar magnitude to g_A , then even the sign of the total “pion-pole” contribution is unknown. The total lattice values of $\gamma_{E1E1}^{(n)}$ are extremely small, so in the absence of a very fine-tuned cancellation between “pion-pole” and structure contributions, it is likely that both are small. We therefore feel justified in placing the lattice points—which include both the physical and pathological pion-pole contributions—on the same plot as our pion-pole-subtracted curves.

In most cases, lattice groups account for the differences between identifying polarisabilities as the terms quadratic in the electromagnetic fields, and the canonical definition via non-pole parts of the Compton amplitudes; see Refs. [59, 83–85] for further discussion. We follow Ref. [86] in adding the Dirac-Foldy contribution of $\alpha_{\text{EM}}(\kappa^{(n)})^2/(4M_N^3) \approx 0.7$ to $\alpha_{E1}^{(n)}$ in Ref. [25]. Similarly, $\alpha_{\text{EM}}/(4M_N^3) \approx 0.2$ should be subtracted from $\beta_{M1}^{(p)}$ at $m_\pi = 806$ MeV in Ref. [18], but the effect is well within the lattice uncertainties [87].

The surprising agreement between some of our chiral curves and lattice results at very large pion masses may be accidental. This agreement occurs far outside the χEFT radius of convergence, and could just be a coincidence. But it is striking, and so we close this section with a testable speculation as to why it could be more than an accident. First we note that, at the order to which we work, the chiral expansion does not produce positive powers of m_π ; our χEFT result includes at most a logarithmic divergence as $m_\pi \rightarrow \infty$. Were we to go further in the expansion, we would encounter the usual problem of contributions that grow with more and more powers of m_π . The very mild dependence on pion mass seen in several lattice observables (see e.g. [72, 73]) can then only be reconciled with χEFT through ever-increasing fine-tuning between terms of different, higher orders. In the case of the lattice polarisabilities for $m_\pi \gtrsim 400$ MeV, such pion-mass-independence is more akin to that expected in a heavy-constituent-quark model, or in the classical Lorentz model which considers heavy, charged particles in a harmonic-oscillator potential. Indeed, this smooth m_π -evolution might be considered generic. Of course, QCD must provide a smooth interpolation between the chiral and heavy-quark regimes; cf. Ref. [88] for the case of baryon masses. It is plausible that results like ours, with weak m_π -dependence at low chiral orders and large pion masses, provide reasonable extrapolations into the regime in which χEFT is *a priori* inapplicable. Such a “principle of chiral persistence” suggests that our chiral extrapolations for the spin polarisabilities may turn out to match future lattice computations at high pion masses, too. If such “chiral persistence” is not a feature of QCD, then those computations will reveal the agreement seen thus far to indeed be accidental.

6 Summary and Conclusions

In this paper, we have presented the static scalar and spin dipole polarisabilities of both the proton and neutron in χEFT as a function of the pion mass. We have included the leading

and sub-leading effects of the nucleon’s pion cloud, together with the leading contributions of the $\Delta(1232)$ and its pion cloud. We have differentiated between two pion-mass regimes. Close to the physical m_π , our results are complete at second order in the small expansion parameter $\delta \approx \sqrt{m_\pi/\Lambda_\chi} \approx \Delta_M/\Lambda_\chi$. This corresponds to three non-vanishing orders for the scalar polarisabilities and two for the spin polarisabilities. For $m_\pi \sim \Delta_M$, however, the results are complete only at leading order since contributions are reordered: leading πN , $\Delta(1232)$ and $\pi\Delta$ effects are all of similar size.

A central goal of the paper is to provide reproducible estimates of uncertainties from within the χ EFT framework which are as objective as feasible. At each pion mass, we have used a recently developed statistical interpretation of standard order-by-order EFT convergence estimates to derive 68% degree-of-belief intervals. The resulting probability distributions are non-Gaussian. They are based on several assumptions: the error associated with the first omitted term in the χ EFT series dominates the uncertainty; the corresponding EFT coefficient is “natural” in units of the breakdown scale; and the size of this first omitted term grows linearly with m_π . The inclusion of select higher-order effects indicates that for pion masses below about 250 MeV our uncertainties are, if anything, overestimated. In fact, basic physical arguments imply that our truncation-error for $\alpha_{E1} + \beta_{M1}$ is markedly too large for $m_\pi > m_\pi^{\text{phys}}$, so we somewhat arbitrarily assign zero truncation error to it. Truncation errors must be combined with uncertainties in the input parameters, like the error on $\alpha_{E1} + \beta_{M1}$ from the Baldin sum rule. A framework that combines all these errors in a statistically consistent way is under development [41, 62].

At the physical pion mass, the truncation errors of the spin polarisabilities augment our previously published prediction of the central values, and our recent fits of the scalar polarisabilities. In all cases, the Bayesian method provides a rigorous theory error. Our spin polarisabilities agree well, within their errors, with available extractions from data, and with the predictions of both dispersion relations and a formulation of χ EFT with relativistic baryons.

For the neutron electric polarisability and $\gamma_{E1E1}^{(n)}$, agreement between our χ EFT predictions and extant lattice computations at $m_\pi \lesssim 350$ MeV is remarkably good. Beyond this pion mass, there are doubts about the convergence of χ EFT, and the error bars we derived are certainly not trustworthy. Nevertheless, if we extrapolate the central value of our χ EFT curves into this regime, agreement persists for lattice results on both $\alpha_{E1}^{(n)}$ and $\alpha_{E1}^{(p)}$ at $m_\pi \approx 400$ MeV—within the uncertainties on the lattice numbers. Taking such an extrapolation for the isovector magnetic polarisability out to $m_\pi \approx 800$ MeV yields striking agreement with the recent results of Ref. [18]. This is surprising, given that χ EFT is certainly not convergent at such a large pion mass. We speculate that such an extrapolation of the χ EFT curve does better than we have any right to expect, because—at the order to which we work—the pion-mass dependence is tame enough to permit smooth evolution into the functional dependence of a constituent-quark model.

While most of the present lattice results are at too high a pion mass to be reliably extrapolated to the physical point, they still corroborate important aspects of our findings. A cancellation between πN loops and short-distance mechanisms encoded in LECs makes the magnetic scalar and spin polarisabilities small at m_π^{phys} , but this cancellation does not persist

away from the physical point. Similar fine-tuning leads to a physical-world proton-neutron difference that, for both the scalar electric and magnetic polarisabilities, is consistent with zero within present uncertainties. Both of these proton-neutron degeneracies are lifted away from the physical point. In the near future, lattice calculations could examine the onset of these cancellations as m_π is lowered towards, and even below, 250 MeV. We pointed out that $\beta_{M1}^{(v)}$ may have a previously-neglected impact on the variation of the proton-neutron mass difference with the quark mass. The critical role of the neutron lifetime in Big-Bang Nucleosynthesis then suggests an anthropic argument may explain what otherwise appears to be a coincidentally small value of $\beta_{M1}^{(v)}$.

Finally, we look forward to a next-order calculation of the polarisabilities in χ EFT. This includes subleading effects of the pion cloud around the Delta. The associated LECs in the χ EFT with an explicit $\Delta(1232)$ are, in principle, constrained by data from other processes, e.g. π N scattering and pion photoproduction. But in practice, their values have non-negligible uncertainties [89–91]. Still, such an $\mathcal{O}(e^2\delta^5)$ calculation could yield more accurate predictions at the physical point, in particular for spin polarisabilities and isovector parts. It may also allow a better assessment of the convergence of the chiral series for $m_\pi \sim \Delta_M$, where only leading-order accuracy is available at present.

Acknowledgements

This project was prompted by a request from A. Alexandru. We are indebted to him and to M. Lujan for discussions and encouragement; to M. Savage for well-timed advice, crucial inspiration, and sharing findings of the NPLQCD collaboration prior to publication; and to S. Beane for discussions on the behaviour of low-energy quantities outside the chiral regime. We also gratefully acknowledge correspondence with A. Alexandru, M. Engelhardt and B. Tiburzi concerning details of their respective lattice computations, and with M. Hoferichter and H. Leutwyler on the impact of $\beta_{M1}^{(v)}$ on the proton-neutron mass difference. Finally, we are grateful to the organisers and participants of the workshops COMPTON SCATTERING OFF PROTONS AND LIGHT NUCLEI: PINNING DOWN THE NUCLEON POLARIZABILITIES (2013) and LATTICE NUCLEI, NUCLEAR PHYSICS AND QCD—BRIDGING THE GAP (2015), both at the ECT*, Trento (Italy), and BOUND STATES AND RESONANCES IN EFFECTIVE FIELD THEORIES AND LATTICE QCD CALCULATIONS, Benasque (Spain, 2014) for financial support, and stimulating presentations and atmosphere. This work was supported in part by UK Science and Technology Facilities Council grants ST/J000159/1 and ST/L005794/1 (JMcG), by the US Department of Energy under contracts DE-FG02-93ER-40756 (DRP), as well as DE-FG02-95ER-40907 and DE-SC0015393 (HWG), and by the Dean’s Research Chair programme of the Columbian College of Arts and Sciences of The George Washington University (HWG).

References

- [1] H. W. Griesshammer, J. A. McGovern, D. R. Phillips and G. Feldman, Prog. Part. Nucl. Phys. **67** (2012) 841 [arXiv:1203.6834 [nucl-th]].
- [2] E. E. Jenkins and A. V. Manohar, In *Effective field theories of the standard model*, 113 (proceedings Dobogokoe 1991, ed. by U.-G. Meißner, World Scientific 1992) and Calif. Univ. San Diego report No. UCSD-PTH 91-30 (91/10, rec. Dec.) 26 p. (201392).
- [3] V. Bernard, N. Kaiser and U.-G. Meißner, Phys. Rev. Lett. **67** (1991) 1515.
- [4] V. Bernard, N. Kaiser and U.-G. Meißner, Int. J. Mod. Phys. E **4** (1995) 193 [arXiv:hep-ph/9501384].
- [5] M. N. Butler and M. J. Savage, Phys. Lett. B **294** (1992) 369 [hep-ph/9209204].
- [6] T. R. Hemmert, B. R. Holstein and J. Kambor, Phys. Lett. B **395** (1997) 89 [hep-ph/9606456].
- [7] T. R. Hemmert, B. R. Holstein and J. Kambor, J. Phys. G **24** (1998) 1831 [hep-ph/9712496].
- [8] V. Pascalutsa and D. R. Phillips, Phys. Rev. C **67** (2003) 055202. [nucl-th/0212024].
- [9] R. P. Hildebrandt, H. W. Griesshammer, T. R. Hemmert and B. Pasquini, Eur. Phys. J. A **20** (2004) 293 [arXiv:nucl-th/0307070].
- [10] J. A. McGovern, D. R. Phillips and H. W. Griesshammer, Eur. Phys. J. A **49** (2013) 12 [arXiv:1210.4104 [nucl-th]].
- [11] L. S. Myers *et al.* [COMPTON@MAX-lab Collaboration], Phys. Rev. Lett. **113** (2014) 262506 [arXiv:1409.3705 [nucl-ex]].
- [12] H. R. Weller, M. W. Ahmed, H. Gao, W. Tornow, Y. K. Wu, M. Gai and R. Miskimen, Prog. Part. Nucl. Phys. **62** (2009) 257.
- [13] HIγS Programme-Advisory Committee Reports 2009 to 2016, with list of approved experiments at www.tunl.duke.edu/higs/experiments/approved/
- [14] E. J. Downie and H. Fonvieille, Eur. Phys. J. ST **198** (2011) 287 [arXiv:1106.0232 [nucl-ex]].
- [15] G. M. Huber and C. Collicott, in: 12TH CONFERENCE ON THE INTERSECTIONS OF NUCLEAR AND PARTICLE PHYSICS (CIPANP 2015), Vail (USA), May 2015, eConf C15-05-19 (2015) [arXiv:1508.07919 [nucl-ex]].
- [16] L. Myers, J. Annand, J. Brudvik, G. Feldman, K. Fissum, H. Griesshammer, K. Hansen and S. Henshaw *et al.* [COMPTON@MAX-lab Collaboration], Phys. Rev. C **92** (2015) 025203 [arXiv:1503.08094 [nucl-ex]].

- [17] P. P. Martel *et al.* [A2 Collaboration], Phys. Rev. Lett. **114** (2015) 112501 [arXiv:1408.1576 [nucl-ex]].
- [18] E. Chang *et al.* [NPLQCD Collaboration], Phys. Rev. D **92** (2015) 114502 [arXiv:1506.05518 [hep-lat]].
- [19] M. Lujan, A. Alexandru, W. Freeman and F. Lee, PoS LATTICE **2014** (2014) 153 [arXiv:1411.0047 [hep-lat]].
- [20] W. Detmold, B. C. Tiburzi and A. Walker-Loud, Phys. Rev. D **81** (2010) 054502 [arXiv:1001.1131 [hep-lat]].
- [21] T. Primer, W. Kamleh, D. Leinweber and M. Burkardt, Phys. Rev. D **89** (2014) 034508 [arXiv:1307.1509 [hep-lat]].
- [22] J. M. M. Hall, D. B. Leinweber and R. D. Young, Phys. Rev. D **89** (2014) 054511 [arXiv:1312.5781 [hep-lat]].
- [23] M. Engelhardt, PoS LATTICE **2011** (2011) 153 [arXiv:1111.3686 [hep-lat]].
- [24] M. Engelhardt [LHPC Collaboration], Phys. Rev. D **76** (2007) 114502 [arXiv:0706.3919 [hep-lat]].
- [25] M. Engelhardt, PoS LAT **2009** (2009) 128 [arXiv:1001.5044 [hep-lat]].
- [26] M. Engelhardt, J. Saenz and R. Höllwieser, private communication and forthcoming.
- [27] W. Freeman, A. Alexandru, M. Lujan and F. X. Lee, Phys. Rev. D **90** (2014) 054507 [arXiv:1407.2687 [hep-lat]].
- [28] H. W. Griebhammer, A. I. L’vov, J. A. McGovern, V. Pascalutsa, B. Pasquini and D. R. Phillips, arXiv:1409.1512 [nucl-th].
- [29] A. Walker-Loud, C. E. Carlson and G. A. Miller, Phys. Rev. Lett. **108** (2012) 232301 [arXiv:1203.0254 [nucl-th]].
- [30] A. Walker-Loud, C. E. Carlson and G. A. Miller, PoS LATTICE **2012** (2012) 136 [arXiv:1210.7777 [hep-lat]].
- [31] F. B. Erben, P. E. Shanahan, A. W. Thomas and R. D. Young, Phys. Rev. C **90** (2014) 065205 [arXiv:1408.6628 [nucl-th]].
- [32] A. W. Thomas, X. G. Wang and R. D. Young, Phys. Rev. C **91** (2015) 015209 [arXiv:1406.4579 [nucl-th]].
- [33] J. Gasser, M. Hoferichter, H. Leutwyler and A. Rusetsky, Eur. Phys. J. C **75** (2015) 375 [arXiv:1506.06747 [hep-ph]].
- [34] K. Pachucki, Phys. Rev. A **60** (1999) 3593.

- [35] C. E. Carlson and M. Vanderhaeghen, arXiv:1109.3779 [physics.atom-ph].
- [36] R. Pohl, R. Gilman, G. A. Miller and K. Pachucki, Ann. Rev. Nucl. Part. Sci. **63** (2013) 175 [arXiv:1301.0905 [physics.atom-ph]].
- [37] V. Lensky and J. A. McGovern, Phys. Rev. C **89** (2014) 032202 [arXiv:1401.3320 [nucl-th]].
- [38] H. W. Griesshammer, J. A. McGovern and D. R. Phillips, forthcoming.
- [39] M. Cacciari and N. Houdeau, JHEP **1109** (2011) 039 [arXiv:1105.5152 [hep-ph]].
- [40] R. J. Furnstahl, N. Klco, D. R. Phillips and S. Wesolowski, Phys. Rev. C **92** (2015) 024005 [arXiv:1506.01343 [nucl-th]].
- [41] R. J. Furnstahl, D. R. Phillips and S. Wesolowski, J. Phys. G **42** (2015) 034028 [arXiv:1407.0657 [nucl-th]].
- [42] D. Babusci, G. Giordano, A. I. L'vov, G. Matone and A. M. Nathan, Phys. Rev. C **58** (1998) 1013 [arXiv:hep-ph/9803347].
- [43] H. W. Griesshammer, *High-Accuracy Analysis of Compton Scattering in Chiral EFT; Status and Future*, invited seminar, A2/CRYSTALL-BALL COLLABORATION MEETING 2013, Institut für Kernphysik, Johannes-Gutenberg-Universität Mainz, Mainz (Germany), 4-5 July 2013; talk, workshop on COMPTON SCATTERING OFF PROTONS AND LIGHT NUCLEI: PINNING DOWN THE NUCLEON POLARISABILITIES, ECT*, Trento (Italy), 29 July-2 August 2013.
- [44] M. C. M. Rentmeester, R. G. E. Timmermans, J. L. Friar and J. J. de Swart, Phys. Rev. Lett. **82** (1999) 4992 [nucl-th/9901054].
- [45] V. Bernard, N. Kaiser, A. Schmidt and U.-G. Meißner, Phys. Lett. B **319** (1993) 269 [hep-ph/9309211].
- [46] K. B. Vijaya Kumar, J. A. McGovern and M. C. Birse, Phys. Lett. B **479** (2000) 167 [hep-ph/0002133].
- [47] V. Olmos de León et al., Eur. Phys. J. A **10** (2001) 207.
- [48] M. I. Levchuk and A. I. L'vov, Nucl. Phys. A **674** (2000) 449 [nucl-th/9909066].
- [49] V. Pascalutsa and D. R. Phillips, Phys. Rev. C **68** (2003) 055205 [nucl-th/0305043].
- [50] T. R. Hemmert, B. R. Holstein and J. Kambor, Phys. Rev. D **55** (1997) 5598 [hep-ph/9612374].
- [51] T. R. Hemmert, B. R. Holstein, J. Kambor and G. Knochlein, Phys. Rev. D **57** (1998) 5746 [nucl-th/9709063].

- [52] V. Lensky, J. McGovern and V. Pascalutsa, Eur. Phys. J. C **75** (2015) 604 [arXiv:1510.02794 [hep-ph]].
- [53] J. Ahrens *et al.* [GDH and A2 Collaborations], Phys. Rev. Lett. **87** (2001) 022003 [hep-ex/0105089].
- [54] H. Dutz, K. Helbing, J. Krimmer, T. Speckner and G. Zeitler [GDH and A2 Collaborations], Phys. Rev. Lett. **91** (2003) 192001.
- [55] M. Camen *et al.*, Phys. Rev. C **65** (2002) 032202.
- [56] B. R. Holstein, D. Drechsel, B. Pasquini and M. Vanderhaeghen, Phys. Rev. C **61** (2000) 034316 [arXiv:hep-ph/9910427].
- [57] B. Pasquini, private communication based on Ref. [9].
- [58] B. Pasquini, P. Pedroni and D. Drechsel, Phys. Lett. B **687** (2010) 160 [arXiv:1001.4230 [hep-ph]].
- [59] M. Schumacher, Prog. Part. Nucl. Phys. **55** (2005) 567 [arXiv:hep-ph/0501167].
- [60] K. Kossert, M. Camen, F. Wissmann, J. Ahrens, J. R. M. Annand, H. J. Arends, R. Beck and G. Caselotti *et al.*, Eur. Phys. J. A **16** (2003) 259 [nucl-ex/0210020].
- [61] M. R. Schindler and D. R. Phillips, Annals Phys. **324** (2009) 682 [arXiv:0808.3643 [hep-ph]]; erratum, Annals Phys. **324** (2009) 2051.
- [62] S. Wesolowski, N. Klco, R. J. Furnstahl, D. R. Phillips and A. Thapaliya, arXiv:1511.03618 [nucl-th].
- [63] E. Epelbaum, H. Krebs and U.-G. Meißner, Eur. Phys. J. A **51** (2015) 53 [arXiv:1412.0142 [nucl-th]].
- [64] E. Epelbaum, H. Krebs and U.-G. Meißner, Phys. Rev. Lett. **115** (2015) 122301 [arXiv:1412.4623 [nucl-th]].
- [65] S. Binder *et al.*, arXiv:1505.07218 [nucl-th].
- [66] H. W. Griesshammer and G. Rupak, Phys. Lett. B **529** (2002) 57 [nucl-th/0012096].
- [67] H. W. Griesshammer, J. A. McGovern and D. R. Phillips, forthcoming.
- [68] M. Procura, B. U. Musch, T. R. Hemmert and W. Weise, Phys. Rev. D **75** (2007) 014503 [hep-lat/0610105].
- [69] J. A. McGovern and M. C. Birse, Phys. Rev. D **74** (2006) 097501 [hep-lat/0608002].
- [70] D. Djukanovic, J. Gegelia and S. Scherer, Eur. Phys. J. A **29** (2006) 337 [hep-ph/0604164].

- [71] M. R. Schindler, D. Djukanovic, J. Gegelia and S. Scherer, Nucl. Phys. A **803** (2008) 68 [arXiv:0707.4296 [hep-ph]].
- [72] A. Walker-Loud, H.-W. Lin, D. G. Richards, R. G. Edwards, M. Engelhardt, G. T. Fleming, P. Hagler and B. Musch *et al.*, Phys. Rev. D **79** (2009) 054502 [arXiv:0806.4549 [hep-lat]].
- [73] A. Walker-Loud, PoS CD **12** (2013) 017 [arXiv:1304.6341 [hep-lat]].
- [74] V. Bernard and U. G. Meissner, Phys. Lett. B **639** (2006) 278 [hep-lat/0605010].
- [75] S. Beane, talk at “8th International Workshop on Chiral Dynamics: Theory and Experiment”, Pisa, Italy, 29 June–3 July, 2015.
- [76] V. Lensky and V. Pascalutsa, Eur. Phys. J. C **65** (2010) 195 [arXiv:0907.0451 [hep-ph]].
- [77] S. R. Beane *et al.*, Phys. Rev. Lett. **113** (2014) 252001 [arXiv:1409.3556 [hep-lat]].
- [78] P. F. Bedaque, T. Luu and L. Platter, Phys. Rev. C **83**, 045803 (2011) [arXiv:1012.3840 [nucl-th]].
- [79] T. Blum, R. Zhou, T. Doi, M. Hayakawa, T. Izubuchi, S. Uno and N. Yamada, Phys. Rev. D **82** (2010) 094508 [arXiv:1006.1311 [hep-lat]].
- [80] W. Detmold, B. C. Tiburzi and A. Walker-Loud, Phys. Rev. D **73** (2006) 114505 [hep-lat/0603026].
- [81] B. C. Tiburzi, Phys. Rev. D **89** (2014) 074019 [arXiv:1403.0878 [hep-lat]].
- [82] D. Stump, J. Pumplin, R. Brock, D. Casey, J. Huston, J. Kalk, H. L. Lai and W. K. Tung, Phys. Rev. D **65** (2001) 014012 [hep-ph/0101051].
- [83] A. I. L’vov, Int. J. Mod. Phys. A **8** (1993) 5267.
- [84] M. Bawin and S. A. Coon, Phys. Rev. C **55** (1997) 419 [arXiv:nucl-th/9610028].
- [85] J. W. Lee and B. C. Tiburzi, Phys. Rev. D **90** (2014) 074036 [arXiv:1407.8159 [hep-lat]].
- [86] M. Engelhardt, private communication.
- [87] B. C. Tiburzi, private communication.
- [88] D. B. Leinweber, A. W. Thomas, K. Tsushima and S. V. Wright, Phys. Rev. D **61** (2000) 074502 [hep-lat/9906027].
- [89] G. C. Gellas, T. R. Hemmert, C. N. Ktorides and G. I. Poulis, Phys. Rev. D **60**, 054022 (1999) doi:10.1103/PhysRevD.60.054022 [hep-ph/9810426].
- [90] V. Pascalutsa, M. Vanderhaeghen and S. N. Yang, Phys. Rept. **437**, 125 (2007) doi:10.1016/j.physrep.2006.09.006 [hep-ph/0609004].

- [91] D. L. Yao, D. Siemens, V. Bernard, E. Epelbaum, A. M. Gasparyan, J. Gegelia, H. Krebs and U. G. Meiner, arXiv:1603.03638 [hep-ph].

A Shapes and Profiles of Corridors of Uncertainties

We show in Fig. 11 the pdfs for all polarisabilities at the physical pion mass, and in Fig. 12 the theoretical error corridors of the results for the m_π -dependence of $\alpha_{E1} \pm \beta_{M1}$, γ_0 and γ_π , as detailed in Sect. 3.3.

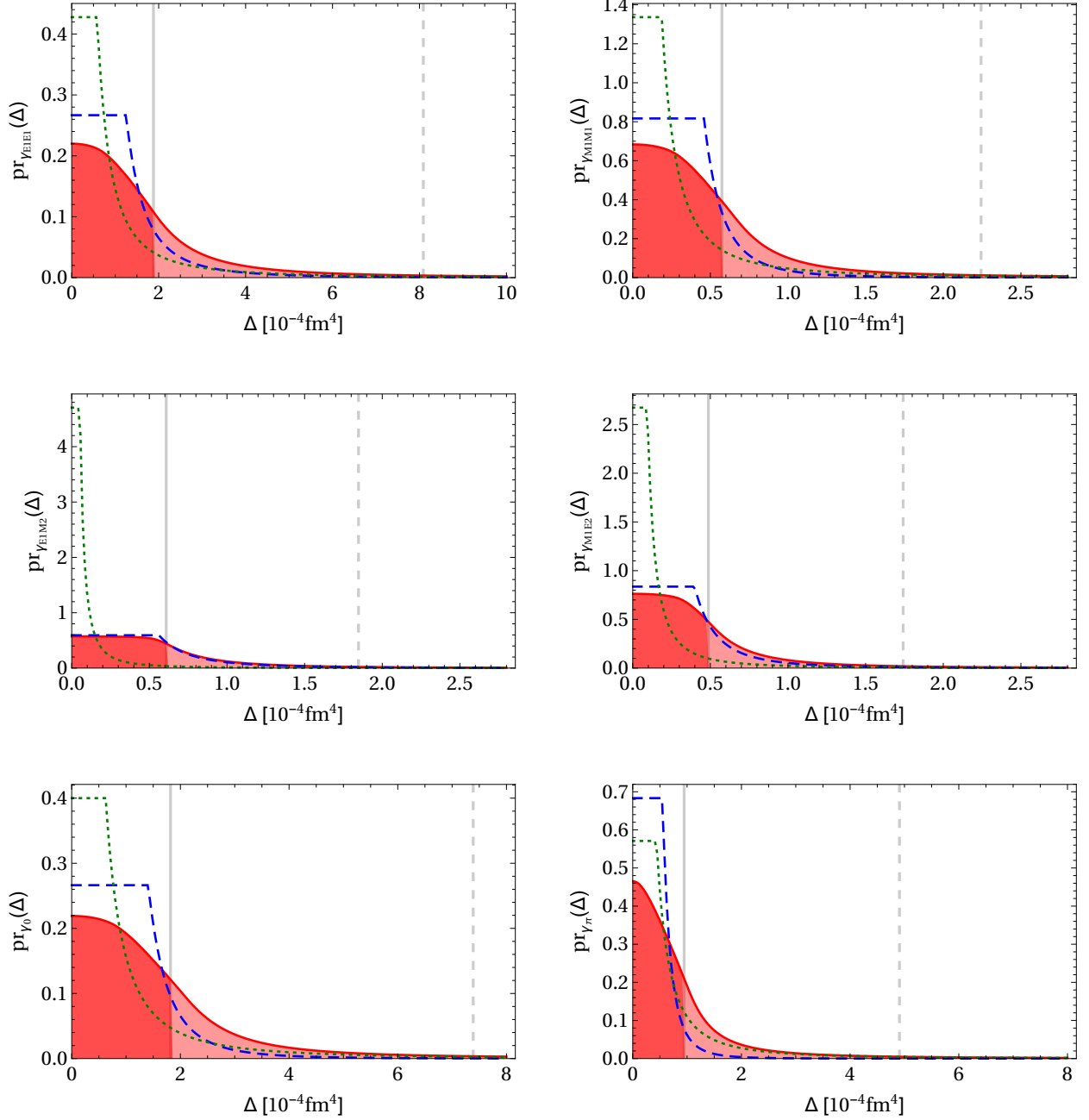


Figure 11: (Colour online) Pdfs for the spin polarisabilities at the physical pion mass. Notation as in Fig. 5.

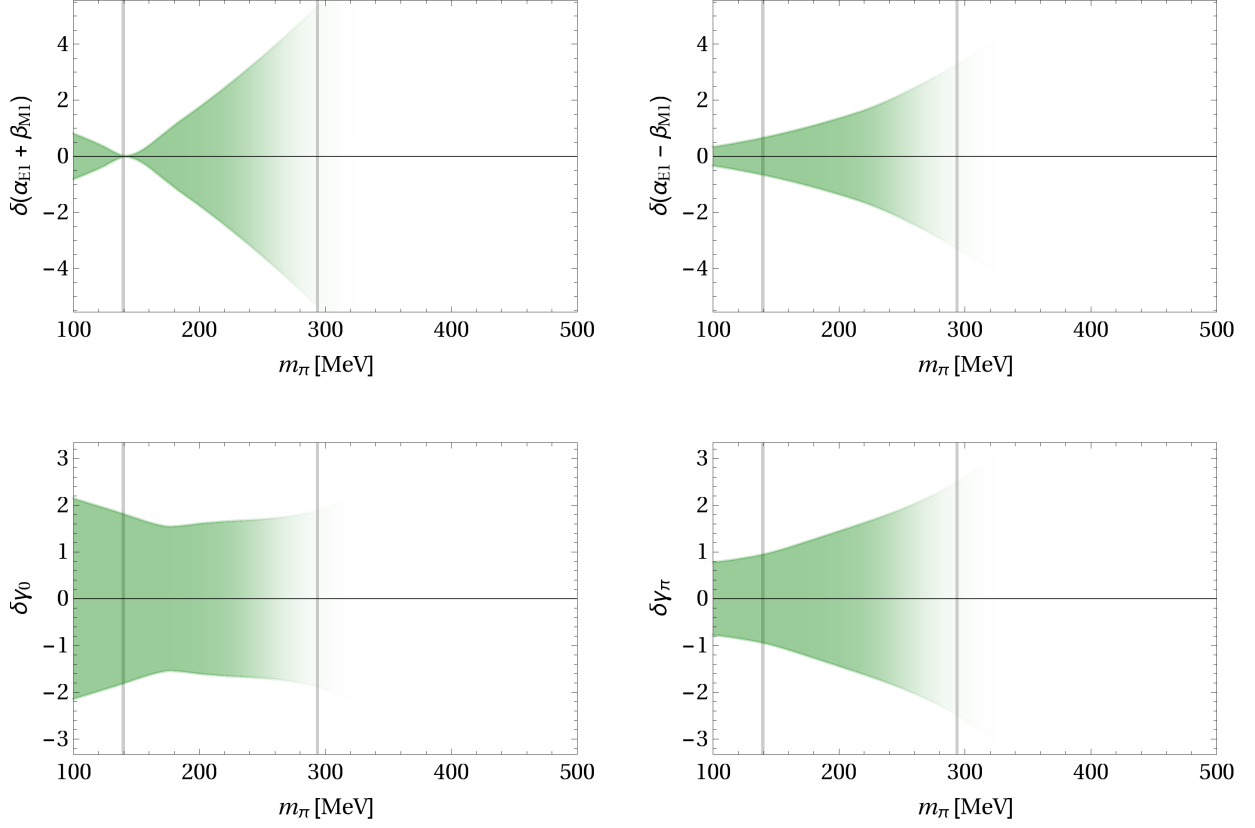


Figure 12: (Colour online) Error bands (68% DoBs) on theoretical results for the m_π -dependence of polarisability combinations $\alpha_{E1} \pm \beta_{M1}$ (top) and $\gamma_{0,\pi}$ (bottom). For γ_π , the original result of the Bayesian analysis is shown. In Fig. 8, it is substituted by that for γ_0 , as detailed in Sect. 3.3.